

RESEARCH ARTICLE

Scutellarein attenuates atopic dermatitis by selectively inhibiting transient receptor potential vanilloid 3 channels

Yujing Wang¹ | Liaoxi Tan¹ | Kejun Jiao¹ | Chu Xue¹ | Qinglian Tang¹ |
Shan Jiang¹ | Younan Ren¹ | Hao Chen² | Tarek Mohamed Abd El-Aziz³ |
Khalid N. M. Abdelazeem⁴ | Ye Yu⁵ | Fang Zhao¹ | Michael X. Zhu⁶  |
Zhengyu Cao¹ 

¹State Key Laboratory of Natural Medicines and Department of TCM Pharmacology, School of Traditional Chinese Pharmacy, China Pharmaceutical University, Nanjing, China

²Institute of Dermatology, Chinese Academy of Medical Sciences & Peking Union Medical College, Nanjing, China

³Zoology Department, Faculty of Science, Minia University, El-Minia, Egypt

⁴Radiation Biology Research Department, National Centre for Radiation Research and Technology, Atomic Energy Authority, Cairo, Egypt

⁵Department of Basic Medicine, School of Basic Medicine and Clinic Pharmacy, China Pharmaceutical University, Nanjing, China

⁶Department of Integrative Biology and Pharmacology, McGovern Medical School, The University of Texas Health Science Center at Houston, Houston, Texas, USA

Correspondence

Zhengyu Cao and Fang Zhao, State Key Laboratory of Natural Medicines and Department of TCM Pharmacology, School of Traditional Chinese Pharmacy, China Pharmaceutical University, Nanjing 211198, China.

Email: zycao@cpu.edu.cn and zhaofang0927@cpu.edu.cn

Ye Yu, Department of Basic Medicine, School of Basic Medicine and Clinic Pharmacy, China Pharmaceutical University, Nanjing 211198, China.

Email: yuye@cpu.edu.cn

Funding information

Joint Project between China Pharmaceutical University and East South University, Grant/Award Number: 2242019K3DZ01; National Science and Technology Major Projects for “Major New Drugs Innovation and Development”, Grant/Award Number: 2018ZX09101003-004-002; National Natural Science Foundation of China, Grant/Award Numbers: 21777192, 81972960, 82100585

Background and Purpose: Atopic dermatitis (AD) is one of the most common chronic inflammatory cutaneous diseases with unmet clinical needs. As a common ingredient found in several medicinal herbs with efficacy on cutaneous inflammatory diseases, Scutellarein (Scu) has been shown to possess anti-inflammatory and anti-proliferative activities. We aimed to evaluate the therapeutic efficacy of Scu against AD and its underlying molecular mechanism.

Experimental Approach: Efficacy of Scu on AD was evaluated in 2,4-dinitrofluorobenzene (DNFB) and carvacrol-induced dermatitis mouse models. Cytokine mRNA and serum IgE levels were examined using qPCR and ELISA, respectively. Voltage clamp recordings were used to measure currents mediated by transient receptor potential (TRP) channels. In silico docking, site-direct mutagenesis, and covalent modification were used to explore the binding pocket of Scu on TRPV3.

Key Results: Subcutaneous administration of Scu efficaciously suppresses DNFB and carvacrol-induced pruritus, epidermal hyperplasia and skin inflammation in wild type mice but has no additional benefit in *Trpv3* knockout mice in the carvacrol model. Scu is a potent and selective TRPV3 channel allosteric negative modulator with an apparent affinity of 1.18 μM . Molecular docking coupled with site-direct mutagenesis and covalent modification of incorporated cysteine residues demonstrate that Scu targets the cavity formed between the pore helix and transmembrane helix S6. Moreover, Scu attenuates endogenous TRPV3 activity in human keratinocytes and inhibits carvacrol-induced proliferative and proinflammatory responses.

Abbreviations: 2-APB, 2-aminoethoxydiphenyl borate; AD, atopic dermatitis; DNFB, 2,4-dinitrofluorobenzene; DTNB, dithiobisnitrobenzoic acid; DTT, dithiothreitol; OS, Olmsted Syndrome; PBMCs, peripheral blood mononuclear cells; P_o , open probability; Scu, scutellarein; TRPV3, transient receptor potential vanilloid 3; TSLP, thymic stromal lymphopoietin.

Yujing Wang and Liaoxi Tan should be considered joint first authors.

Conclusion and Implications: Collectively, these data demonstrate that Scu ameliorates carvacrol-induced skin inflammation by directly inhibiting TRPV3, and TRPV3 represents a viable therapeutic target for AD treatment.

KEYWORDS

atopic dermatitis, keratinocytes, scutellarein, TRPV3

1 | INTRODUCTION

Atopic dermatitis (AD), the most common chronic inflammatory cutaneous disease, affects approximately 10%–17% children and 1%–7% adults in USA (Vakharia & Silverberg, 2019). The pathogenesis of AD is complex and multifactorial. Interactions between genetic susceptibility and multiple environmental factors contribute to the progressive pathophysiology of AD (Sánchez-Borges et al., 2019). The immunological response of AD initiates with an activation of Th2/Th22 pathways that increases immunoglobulin E (IgE) production with subsequent activation of Th1 and Th17 pathways (Werfel et al., 2016). Pathologically, AD is characterized by thickening, redness, scaling, and intense pruritus in the skin lesion (Kapur et al., 2018). The high level of serum IgE and overexpression of proinflammatory mediators, such as **tumour necrosis factor-alpha** (TNF- α), **interleukin-1 β** (IL-1 β), **IL-4**, **IL-6**, and **IL-8**, in the skin lesion are considered as key molecular markers of AD (Möbus et al., 2021; Werfel et al., 2016). Topical application of corticosteroids and calcineurin inhibitors, phototherapy, and systemic immunosuppressants are commonly used in the clinics for AD therapy (Langan et al., 2020). However, these treatments have significant adverse effects including skin atrophy and increased risk for lymphoma and non-melanoma skin cancer development (Langan et al., 2020). Therefore, there is an urgent need for alternative treatment options for AD.

Transient receptor potential vanilloid 3 (**TRPV3**) is a polymodal Ca²⁺-permeable non-selective cation channel abundantly expressed in the dorsal root ganglia (Xu et al., 2002), skin keratinocytes (Peier et al., 2002), nasal and oral epithelial cells (Aijima et al., 2015; Xu et al., 2006), where they participate in a plethora of physiological functions such as skin barrier formation, keratinocyte proliferation (Cheng et al., 2010; Wang et al., 2021), hair follicle formation (Borbíró et al., 2011), and skin inflammation (Szöllösi et al., 2018). Humans carrying TRPV3 gain-of-function mutations, mostly Gly573Ser/Cys (TRPV3^{G573S/C}), bear **Olmsted syndrome** (OS) with clinic features of severe itching, skin inflammation, and palmoplantar keratoderma (Lin et al., 2012). Ironically, *WBN/Kob-Ht* rats and *DS-Nh* mice, which carry also gain-of-function mutations, TRPV3^{G573C} and TRPV3^{G573S}, respectively, develop spontaneous dermatitis as well, with increased levels of IgE and **nerve growth factor** (NGF), enhanced mast cells infiltration, and severe itch resembling the clinic features of AD (Asakawa et al., 2005; Imura et al., 2009; Yamamoto-Kasai et al., 2013). In a 2,4-dinitrofluorobenzene (DNFB)-induced AD mouse model, the expression level of TRPV3 is significantly increased whereas deletion of *Trpv3* attenuated DNFB-induced skin pathology (Qu et al., 2019).

What is already known

- Scutellarein (Scu), a common ingredient in several medicinal herbs, possesses anti-inflammatory and anti-proliferative activities.

What does this study add

- Scu ameliorates carvacrol-induced AD through a TRPV3-dependent pathway.
- Scu inhibits TRPV3 by binding to the cavity formed by S6 helix and pore helix.

What is the clinical significance

- TRPV3 represents a viable therapeutic target for AD treatment.
- Scu may represent a novel lead compound for AD therapy.

These studies suggest that TRPV3 represents a key regulator of the progressive pathology of AD.

Carvacrol, one of the main bioactive compounds in the essential oil and widely used in food as a flavouring ingredient and in cosmetic formulations, has been shown to activate certain thermo-sensitive TRP channels, including TRPV3 and **TRPA1** (Suntres et al., 2015; Xu et al., 2006), **ryanodine receptors**, and to inhibit **sarcoplasmic reticulum Ca²⁺ ATPase** (Sárközi et al., 2007). Recent studies have demonstrated that topical application of carvacrol induces itch, hyperplasia, and skin inflammation (Qu et al., 2019; Wang et al., 2021), resembling the clinic features of AD.

Scutellarein (Scu) is one of the main flavonoids of *Scutellaria baicalensis* Georgi, a traditional Chinese medicine widely used to treat respiratory infections, liver inflammation, and skin and epithelial inflammatory diseases (Liao et al., 2021; Zhao et al., 2019). It is also abundant in many other medicinal herbs such as *Oroxylum indicum* (Linn.) Kurz and *Erigeron breviscapus* (vant.) Hand-Mazz, two traditional Chinese medicines widely used for cutaneous inflammatory diseases (Harminder et al., 2011; Wu et al., 2011). Scu has been reported

to possess a wide range of biological activities including anti-inflammatory, antioxidant, anti-virus, and anti-proliferative activities (Chen et al., 2020; Guo et al., 2019; Miao et al., 2020; Sung et al., 2015). It also shows therapeutic potential against idiopathic pulmonary fibrosis, Alzheimer's disease, obesity, and cancer (Chen et al., 2020; Guo et al., 2019; Lin et al., 2019; Miao et al., 2020). However, whether Scu has therapeutic efficacy on AD and its molecular mechanism of action remain elusive.

In the current study, we demonstrated the efficacious protective effect of Scu on cutaneous inflammation in mouse models of AD and determined TRPV3 to be its molecular target. Subcutaneous injection of Scu suppressed the DNFB- and carvacrol-induced pruritus, epidermal hyperplasia and skin inflammatory response in wild type (WT) mice but had no additional benefit in *Trpv3* knockout (KO) mice in the carvacrol model. We showed that Scu directly inhibits TRPV3 activity by targeting a pocket formed between the S6 transmembrane helix and pore helix, providing the molecular mechanism of TRPV3 inhibition by Scu. Finally, Scu inhibited endogenous TRPV3 currents in human skin keratinocytes and suppressed their proliferative and proinflammatory responses.

2 | MATERIALS AND METHODS

2.1 | Animals

All animal experiments were carried out according to the National Institutes of Health guideline for the care and use of laboratory animals (NIH Publications No. 8023, revised 1978) and approved by the Laboratory Animal Management Committee of China Pharmaceutical University (SYXK 2018-0019). The study was designed to generate groups of equal size, and NC3Rs (National Center for Replacement, Refinement and Reduction of Animals) principles were taken into consideration for the sample sizes of animal experiments using randomization and blinded analysis (Kilkenny et al., 2010; McGrath et al., 2015). Animal studies were in compliance with the ARRIVE guidelines (Curtis et al., 2015; Kilkenny et al., 2010; Lilley et al., 2020; McGrath et al., 2015; Percie du Sert et al., 2020) and with the recommendations made by the *British Journal of Pharmacology*. The number of animals and group sizes were calculated by a priori power analysis using G*Power software (version 3.1, Universität Kiel, Kiel, Germany) (Faul et al., 2007) with the following parameters: effect size $f = 0.87$, α (error probability) = 0.05, power (1- β error probability) = 0.8, and number of groups = 4 or 5. The effect size f , as defined by Cohen (1988), was computed from the mean value and sample size of each group and a mean SD value derived from all groups based on our previous experience (Wang et al., 2021). Efforts were made to minimize animal suffering and reduce the number of experimental animals. To investigate Scu effect on DNFB or carvacrol-induced dermatitis, male and female WT C57BL/6J mice (RRID:IMSR_JAX:000664, aged 6–8 weeks, $n = 57$ mice, $n = 5$ or 8/group in different experiments) were obtained from the Animal Core Facility of Nanjing Medical University (Nanjing, China). To investigate the role of TRPV3 on Scu

alleviation of carvacrol-induced AD, age-matched WT ($n = 10$, $n = 5$ /group) and *Trpv3* KO ($n = 10$, $n = 5$ /group) mice (aged 6 weeks) were used and the *Trpv3* KO line was the same as previously described (Wang et al., 2021). All mice were housed at a temperature of $23.0 \pm 2^\circ\text{C}$ with a 12-h light–dark cycle. Food and water were provided ad libitum throughout the experiments.

2.2 | Materials

Carvacrol (Cat# 282197), 2,4-dinitrofluorobenzene (DNFB, Cat# D1529), 2-APB (Cat# D9754), GSK1016790A (GSK, Cat# G0798), allyl isothiocyanate (AITC, Cat# 36682), menthol (Cat# M2772), dexamethasone (Dex, Cat# D1756) and ruthenium red (RR, Cat# R2751) were obtained from Sigma-Aldrich (St. Louis, MO, USA). Scutellarein (Cat# B21479), baicalein (Cat# B20571), chrysin (Cat# B20063), and hispidulin (Cat# B20428) were purchased from Yuanye Biotechnology (Shanghai, China) with purity above 98%. Tribromoethanol (Cat# T161626), and capsaicin (Cat# C107693) was obtained from Aladdin Biochemical Technology Co., Ltd. (Shanghai, China). 5-Bromo-2-deoxyUridine (BrdU, Cat# ED1100) and anti-BrdU antibody (Cat# BM0201) were purchased from BOSTER (Wuhan, Hubei, China). Alexa Fluor 555 conjugated goat anti-mouse IgG (H + L) secondary antibody (Cat# 4409, RRID:AB_1904022) was provided by Cell Signaling Technology (Boston, MA, USA). Methylthiazolyldiphenyl-tetrazolium bromide (MTT, Cat# ST316) was obtained from Beyotime (Shanghai, China). Fluo-4 AM (Cat# R8142) was purchased from Molecular Devices, LLC. (San Jose, CA, USA). Geneticin (G418, Cat# 10131035), blasticidin (Cat# A1113903), hygromycin B (Cat# 10687010), and Dulbecco's Modified Eagle Medium (DMEM, Cat# 11965092) were purchased from Gibco (Grand Island, NY, USA). TRIzol reagent (Cat# R401-01), HiScript II Q RT SuperMix for qPCR (+ gDNA wiper) (Cat# R223-01), and AceQ qPCR SYBR Green Master Mix premixed low ROX (Cat# Q131-02) were provided by Vazyme (Nanjing, Jiangsu, China). Human peripheral blood leukocytes isolation kit (Cat# WBC1077K) was purchased from TBD Science (Tianjin, China). Other inorganic chemicals were purchased from Sigma-Aldrich (St. Louis, MO, USA) and were of the highest grade available.

2.3 | AD mouse models

Repeated administrations of DNFB or carvacrol were used to produce mouse models of AD. DNFB was applied as previously described (Qu et al., 2019). Briefly, after depilation using paraffin, a volume of $100 \mu\text{l}$ 0.5% DNFB (dissolved in acetone/olive oil = 4:1, v/v) was topically smeared onto mouse dorsum at day 1 for sensitization. Starting at day 5, the mouse received topical application of 0.2% DNFB ($50 \mu\text{l}$) once a day for three consecutive days (Figure S1A). Mice in the control group were topically applied with

acetone/olive oil (4:1) solution at the same time of DNFB administration. The skin samples were harvested at day 8 and were either fixed with 4% paraformaldehyde or freshly frozen in liquid nitrogen. To generate carvacrol-induced AD mouse model, 1 day after depilation using paraffin, 2% carvacrol (100 μ l, dissolved in 30% ethanol solution) was topically smeared onto mouse dorsum (once a day, for 5 consecutive days). For control, mice were topically applied with 30% ethanol solution every day for 5 consecutive days. The skin samples were harvested at day 6 and were either fixed with 4% paraformaldehyde or freshly frozen in liquid nitrogen. Before collecting the skin samples, mice were anaesthetised by tribromoethanol (300 mg·kg⁻¹, i.p.) and killed with gradually increased concentration of CO₂ from 30% to 70% over 10 min, followed by blood aspiration from heart. Gross appearance of the dorsal skin was photographed before application of DNFB or carvacrol and the degree of dermatitis was scored according to the severity of the skin erythema, escharosis and thickness. Each property was graded on a scale of 0–4. Erythema was measured using ImageJ as previously described (Logger et al., 2020). The degree of pruritis was calculated by counting scratching bouts in a period of 15 min after application of DNFB or carvacrol. A scratching bout consisted of a series of movements when the mouse lifted its hind limb towards dorsal skin and scratched for any length of time until the limb returned to the floor or mouth. To investigate the drug efficacy against AD, Scu at two doses (0.2 and 0.5 mg·kg⁻¹·day⁻¹) or vehicle solution (saline containing 10% tween-80) at a volume of 5 ml·kg⁻¹ was subcutaneously injected into the dorsum (once a day) at four dispersed sites 30 min before the topical application of DNFB or carvacrol. Subcutaneous administration of 2.5 mg·kg⁻¹ Dex was used as positive control in carvacrol-induced AD mouse model. Individuals who were blinded to the treatment conditions evaluated all animal experiments.

2.4 | Histopathological examination

Excised mouse dorsal skins were fixed in 4% paraformaldehyde overnight, followed by embedding in paraffin. The tissues were sectioned at 2 μ m and stained with haematoxylin and eosin (H&E). Images of the sections were taken at 100 \times using a CCD camera attached to an Eclipse Ti inverted microscopy (RRID:SCR_021242, Nikon, Tokyo, Japan). Epidermal thickness was measured using linear distance tool of NIS-Elements BR software (Nikon, Tokyo, Japan, RRID:SCR_002776).

2.5 | Serum IgE ELISA assay

Whole blood samples were collected from the mice after killing. Serum samples were obtained after centrifugation (3500 rpm, 10 min) and stored at –80°C until quantitative analysis. Serum IgE concentration was quantified using a murine IgE ELISA kit (Cat# E-EL-M3034, Elabscience Biotechnology Co., Ltd, Wuhan, China) according to the manufacturer's instruction.

2.6 | RNA extraction and real-time quantitative PCR

The total RNA was extracted using TRIzol reagent and reverse-transcribed to cDNA using HiScript II Q RT SuperMix for qPCR (+gDNA wiper) as described previously (Wang et al., 2021). Primers (sequences listed in Table S1) were synthesized by TsingKe Biological Technology (Nanjing, Jiangsu, China). Real-time quantitative PCR (qPCR) was carried out with AceQ qPCR SYBR Green Master Mix premixed with low ROX in a QuantStudio 3 Real-Time PCR System (RRID:SCR_018712, Thermo Fisher Scientific, Waltham, MA, USA). The relative mRNA expression was calculated using the comparative Ct (2^{– $\Delta\Delta$ Ct}) method, and was normalized to that of GAPDH.

2.7 | Cell cultures

HaCaT cells (RRID:CVCL_0038) were maintained in DMEM supplemented with 10% fetal bovine serum (FBS) and 1% penicillin-streptomycin (P/S). HEK-293 cells stably expressing human (h)TRPV1, mouse (m)TRPV2, mTRPV3, hTRPV4, hTRPM8, or hTRPA1 were generated in our lab as previously described (Zhao et al., 2021). HEK-293 cells expressing hTRPV1, mTRPV2, mTRPV3, or hTRPV4 were maintained in DMEM supplemented with 10% FBS, 1% P/S and 500 μ g·ml⁻¹ G418 whereas HEK-293 cells expressing hTRPA1 or hTRPM8 were maintained in DMEM supplemented with 10% FBS, 1% P/S, 5 μ g·ml⁻¹ blasticidin and 50 μ g·ml⁻¹ hygromycin B. All cells were incubated at 37°C in a humidified incubator with 5% CO₂.

2.8 | Electrophysiology

Electrophysiological recordings of individual subtypes of TRP channels expressed in HEK-293 cells were performed at room temperature using an EPC-10 amplifier (RRID:SCR_018399, HEKA Elektronik, Lambert/Pfalz, Germany) controlled by the PatchMaster software (RRID:SCR_000034, HEKA Elektronik, Lambert/Pfalz, Germany). Recording pipettes were pulled from borosilicate glass using P-1000 Micropipette Puller (Sutter Instrument, Novato, CA, USA) to 3–5 M Ω (whole-cell recording) and ~10 M Ω (inside-out or outside-out recording) when filled with a pipette solution containing (in mM): 140 CsCl, 1 MgCl₂, 5 EGTA, 10 HEPES, 0.1 CaCl₂, pH 7.20. The bath solution contained (in mM): 140 NaCl, 5 KCl, 2 CaCl₂, 1 MgCl₂, 10 glucose, and 10 HEPES, pH 7.40. Cells were held at –60 mV and the currents, elicited by a voltage ramp from –100 to +100 mV every 650 ms, were recorded at 5 kHz. For single-channel recordings, currents were sampled at 5 kHz and the membrane potential was held at +60 mV. Single-channel currents were digitally filtered at 100 Hz for display. Compounds were applied through a pressure-driven multichannel system (ALA Scientific Instruments, Farmingdale, NY, USA) with the outlet placed approximately 50 μ m away from the cell being recorded. Single-channel current was identified based on the half-amplitude threshold-crossing criteria. Open probability (NP_o) was calculated as

the ratio of the sum of all open durations to the total trace duration using Clampfit 10 (RRID:SCR_011323, Molecular Devices, Sunnyvale, CA, USA) and the chord conductance of the single channel was determined as the ratio of the current amplitude at level 1 to the membrane potential +60 mV.

2.9 | In silico docking

The cryo-EM structure of mTRPV3 (PDB ID code: 6LGP) was prepared using the Protein Preparation Wizard (RRID:SCR_016749) (Friesner et al., 2006). The small molecule conformations of Scu were prepared using LigPrep (RRID:SCR_016746) (Gadakar et al., 2007). The docking program Glide (RRID:SCR_000187) (Friesner et al., 2004) was employed to dock Scu into the potential binding sites. The grid for the protein was set to 30 Å, and the extra precision (XP) docking mode was selected in in silico docking. All procedures including protein preparation, refinement, grid generation, and docking were carried out using the default parameters. The threshold for rejecting minimized poses was 0.5 kcal·mol⁻¹. Docking scores and Scu-residue interaction scores were summarized, sorted, and then plotted using Maestro (RRID:SCR_016748) (Li et al., 2018). During this docking process, the protein and the Scu were both flexible. All structural figures were made by PyMol (RRID:SCR_000305, <http://www.pymol.org>).

2.10 | Site directed mutagenesis and transient transfection

Mouse *Trpv3* cDNA construct was a gift of Prof. Jie Zheng (University of California, Davis). To facilitate the identification of TRPV3-transfected cells, green fluorescence protein (GFP) was genetically linked to the C terminus of TRPV3. Point mutations were generated using KOD plus mutagenesis kit (Cat# SMK-101, Toyobo, Osaka, Japan). All mutants were confirmed by DNA sequencing. HEK-293 cells (RRID:CVCL_0063) were maintained in DMEM medium supplemented with 10% FBS and 1% P/S. Cells were transiently transfected with cDNA constructs by lipofectamine[®] 2000 according to the manufacturer's protocol. Patch-clamp recordings were performed at 24–30 h after transfection.

2.11 | BrdU-incorporation assays

To identify proliferating cells, a BrdU-incorporation assay was performed as previously described (Wang et al., 2021). In brief, HaCaT cells were seeded in 96-well plates at a density of 5000 cells per well and treated with 100 μM carvacrol in the absence or presence of 10 μM Scu for 12 h. The treated cells were incubated with BrdU for an additional 3 h. Cells were then fixed with 4% paraformaldehyde for 30 min and permeabilized with 0.5% TritonX-100 for 15 min. The DNA was denatured by incubating with 2 M HCl for 30 min at 37°C, followed by the addition of 0.1 M Na₂B₄O₇. After blocking with 5%

BSA, cells were incubated with anti-BrdU antibody (1:400) overnight at 4°C and subsequently incubated with Alexa Fluor 555-conjugated goat anti-mouse secondary antibody for 1 h. Hoechst 33342 was used for labelling nuclei. Pictures were taken using a Leica inverted fluorescence microscope (RRID:SCR_013673, Leica Microsystems, Inc., Buffalo Grove, IL, USA). The experimental detail for conducting immunofluorescence conforms with BJP Guidelines (Alexander et al., 2018).

2.12 | Leukocyte chemotaxis assays

The study was approved (protocol code: 2019-ky013) by the research ethics board of the Institute of Dermatology and Hospital for Skin Diseases, Chinese Academy of Medical Sciences, and informed consent of donors was obtained. Human peripheral blood mononuclear cells (PBMCs) were isolated from healthy donors using a human peripheral blood leukocyte isolation kit according to the manufacturer's instructions. In brief, isolated PBMCs were suspended in RPMI 1640 containing 10% FBS and seeded into a transwell insert placed in a culture chamber (Corning, NY, USA) that contained culture medium harvested from keratinocytes treated with different drugs for 6 h. After culturing for 3 h at 37°C under 5% CO₂, the leukocytes migrated to the bottom side of the 5 μm porosity polycarbonate membrane of the insert were fixed by 10% methanol and stained with 0.1% (w/v) crystal violet for 30 min. After staining, images of the leukocytes were captured using a CCD camera attached to an Eclipse Ti inverted microscopy (Nikon, Tokyo, Japan) controlled by NIS-Elements BR software version 4.3 (Nikon, Tokyo, Japan). The numbers of BrdU-positive cells and PBMCs were manually counted by investigators blinded to the treatment conditions.

2.13 | Statistical analysis

The immuno-related procedures used comply with the recommendations made by the *British Journal of Pharmacology* (Curtis et al., 2018). Declared group sizes represented the number of independent values (one data point per animal, slice, or cell) and all statistical analyses were performed using such independent values (technical replicates were not considered independent values). Statistical analysis was undertaken only for studies where each group size was at least $n = 5$. No data points were excluded from the analysis in any results. For experiments with a smaller sample size (i.e., $n < 5$), data were presented as preliminary observations and were not subjected to statistical analysis in this study.

Data were analysed and plotted using GraphPad Prism 6.0 (RRID:SCR_002798, GraphPad Software, Inc., San Diego, CA, USA). All the data were presented as mean ± SEM. The statistical significance was determined using unpaired Student's *t*-test or one-way ANOVA, and only if *F* in ANOVA achieved *P* value less than 0.05 and there was no significant variance inhomogeneity, a post hoc Dunnett's comparison

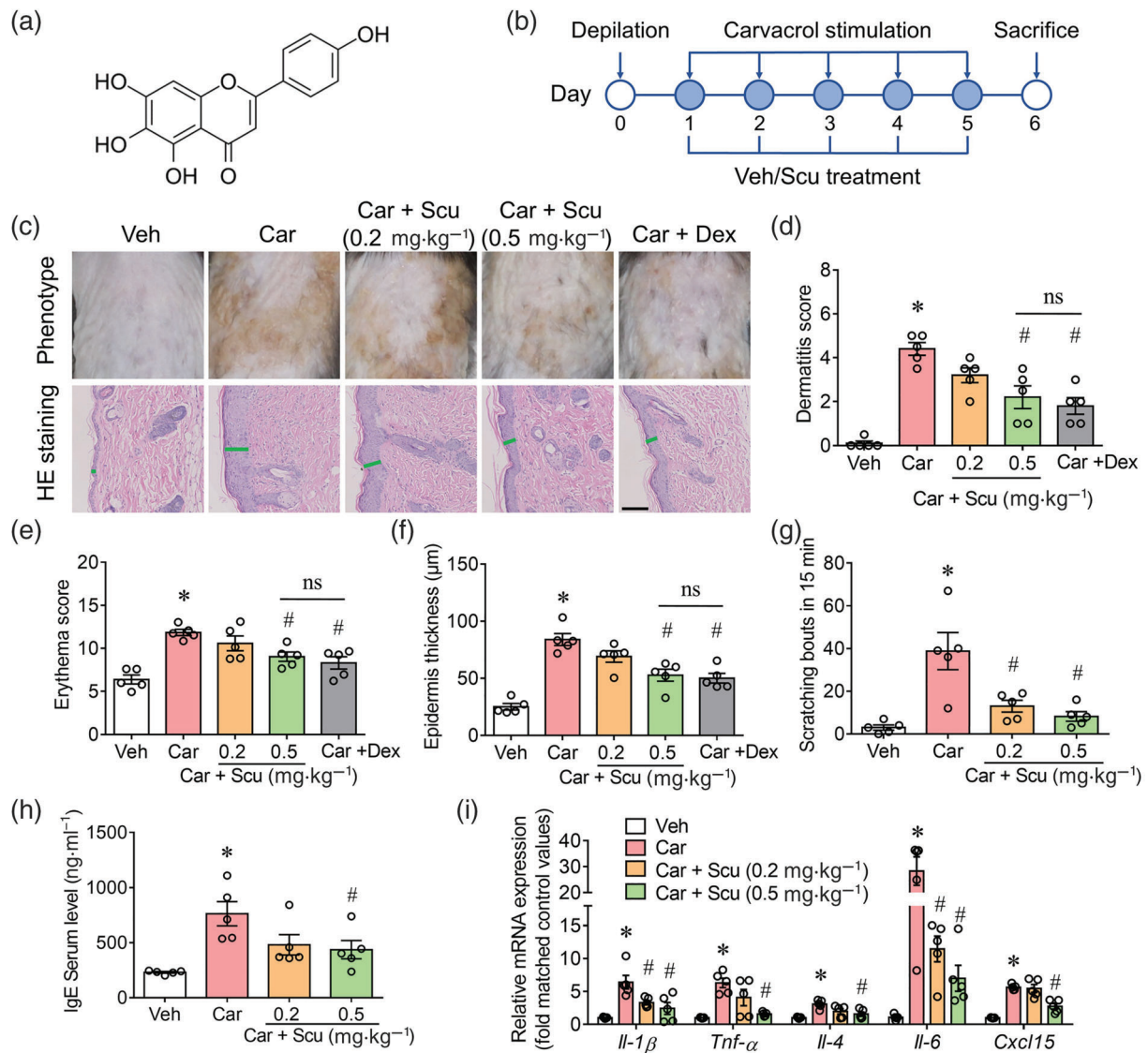


FIGURE 1 Scu alleviates carvacrol-induced dermatitis. (a) The chemical structure of Scu. (b) Schematic illustration depicting the establishment of carvacrol-induced atopic dermatitis mouse model and the administration of Scu (0.2 and 0.5 mg.kg⁻¹). (c) Representative images of the gross appearance (upper panel) and H&E-stained sections (bottom panel) of the back skins of WT C57BL/6J mice treated with vehicle (Veh, 30% ethanol solution and saline containing 10% tween-80), 2% carvacrol (Car), Car plus Scu (0.2 or 0.5 mg.kg⁻¹), and Car plus Dex (2.5 mg.kg⁻¹). Black scale bar, 100 μm. Green lines indicate the thickness of epidermis. (d-f) Quantification of dermatitis score (d), erythema score (e), and epidermal thickness (f) in mice treated with Veh, Car, Car plus Scu, and Car plus Dex. (g, h) Quantification of scratching bouts (g) and serum IgE level (h) in mice treated with Veh, Car, and Car plus Scu. (i) Relative mRNA levels of *Il-1β*, *Tnf-α*, *Il-4*, *Il-6*, and *Cxcl15* in the back skins of the indicated groups, normalized to that of the Veh group. All bar graphs represent mean ± SEM (n = 5 mice). *P < 0.05 versus Veh; #P < 0.05 versus Car, by one-way ANOVA followed by Dunnett's multiple comparison tests

was conducted. A value of $P < 0.05$ was considered statistically significant. All data were tested for normal distribution and equal variance. To quantify the inhibitory effects of Scu on thermosensitive TRP channels, we normalized the currents to each respective control cell to reduce the unwanted sources of variation. Normalized data were analysed using non-parametric Mann-Whitney test. To analyse mRNA expression, data were normalized to vehicle group to reduce variance; y axes were labelled in figures using “fold matched control values.”

Non-linear regression analysis was used to fit concentration-response curves.

2.14 | Nomenclature of targets and ligands

Key protein targets and ligands in this article are hyperlinked to corresponding entries in <http://www.guidetopharmacology.org>, and are

permanently archived in the Concise Guide to PHARMACOLOGY 2021/22 (Alexander & Mathie, 2021).

3 | RESULTS

3.1 | Scu alleviates carvacrol and DNFB-induced dermatitis

To examine the effect of Scu (Figure 1a) on skin inflammatory disease, we first used a mouse AD model produced by topical application of 2% carvacrol once a day for five consecutive days (Figure 1b). This treatment in WT C57BL/6J mice evoked inflamed and scaly skin lesions (Figure 1c, upper panel) and remarkable acanthosis as shown by the increased epidermal thickness in H&E-staining (Figure 1c, bottom panel). Subcutaneous injection of Scu at doses of 0.2 and 0.5 mg·kg⁻¹ to the dorsum at four dispersed sites each day before the topical application of carvacrol markedly attenuated the skin lesion, erythema, and acanthosis (Figure 1c). With 0.2 and 0.5 mg·kg⁻¹ Scu, dermatitis scores were reduced by 27.9 ± 7.9% (n = 5, P > 0.05) and 51.2 ± 12.0% (n = 5, P < 0.05), erythema scores were suppressed by 23.2 ± 15.8% (n = 5, P > 0.05) and 51.6 ± 9.9% (n = 5, P < 0.05), and epidermal thicknesses were reduced by 25.3 ± 8.4% (n = 5, P > 0.05) and 53.1 ± 9.0% (n = 5, P < 0.05), respectively (Figure 1d–f). The positive control, Dex (2.5 mg·kg⁻¹) decreased carvacrol-induced dermatitis scores by 60.5 ± 8.7% (n = 5, P < 0.05), erythema scores by 64.8 ± 13.0% (n = 5, P < 0.05) and epidermal thickness by 57.6 ± 7.2% (n = 5, P < 0.05) (Figure 1d–f). The carvacrol treatment also evoked pruritus, as indicated by the increased number of scratching bouts from 3.0 ± 1.2 to 38.8 ± 8.7 per 15 min (n = 5, P < 0.05), and Scu dose-dependently decreased the carvacrol-evoked pruritus by 72.1 ± 6.2% (0.2 mg·kg⁻¹ Scu, n = 5, P < 0.05) and 85.5 ± 5.1% (0.5 mg·kg⁻¹ Scu, n = 5, P < 0.05) (Figure 1g). Moreover, the carvacrol-treated mice displayed significantly increased serum IgE levels (762.7 ± 110.2 ng·ml⁻¹) as compared with the vehicle-treated ones (230.3 ± 7.6 ng·ml⁻¹, n = 5, P < 0.05), and Scu (0.5 mg·kg⁻¹) significantly decreased the effect of carvacrol by 61.3 ± 15.6% (n = 5, P < 0.05) (Figure 1h). Finally, supporting an inflammatory response, the carvacrol treatment significantly increased the mRNA levels of *Il-1β*, *Tnf-α*, *Il-4*, *Il-6*, and *Cxcl15* in the skin lesions, which were again attenuated by Scu, at least at 0.5 mg·kg⁻¹ (Figure 1i).

We also investigated Scu effect on a more commonly used AD mouse model induced by DNFB (Figure S1A). Repeated application of DNFB evoked severe dermatitis, swelling and erythema (Figure S1B, upper panel) and remarkable acanthosis as demonstrated by H&E-staining (Figure S1B, bottom panel). Subcutaneous injection of Scu dose-dependently suppressed DNFB-induced dermatitis (Figure S1C), erythema (Figure S1D), and epidermis hyperplasia (Figure S1E). At 0.5 mg·kg⁻¹·day⁻¹, Scu reduced DNFB-induced dermatitis score, erythema, and epidermal thickness by 48.5 ± 5.2% (n = 8, P < 0.05) (Figure S1C), 64.3 ± 7.2% (n = 8, P < 0.05) (Figure S1D), and 50.3 ± 7.5% (n = 8, P < 0.05) (Figure S1E), respectively. The DNFB treatment also increased the number of scratching bouts from 2.12 ± 0.52

to 10.25 ± 2.12 per 15 min (n = 8, P < 0.05), and Scu dose-dependently suppressed the DNFB-evoked pruritus by 59.8 ± 21.4% (0.2 mg·kg⁻¹ Scu, n = 8, P > 0.05) and 96.6 ± 11.1% (0.5 mg·kg⁻¹ Scu, n = 8, P < 0.05) (Figure S1F). Moreover, DNFB treatment increased serum IgE level from 164.5 ± 15.5 ng·ml⁻¹ to 586.9 ± 56.3 ng·ml⁻¹ (n = 8, P < 0.05), and Scu dose-dependently decreased the DNFB-evoked increase in serum IgE level by 80.8 ± 7.3% (0.2 mg·kg⁻¹ Scu, n = 8, P < 0.05) and 91.3 ± 5.1% (0.5 mg·kg⁻¹ Scu, n = 8, P < 0.05) (Figure S1G). These results demonstrate that Scu can alleviate the pathological hallmarks of AD in both carvacrol and DNFB-induced AD mouse models.

3.2 | Scu attenuation of carvacrol-induced dermatitis is dependent on TRPV3

Because carvacrol is a nonspecific TRPV3 agonist (Xu et al., 2006), we evaluated the role of TRPV3 in the carvacrol-induced dermatitis and the protective effect of Scu using the *Trpv3*^{-/-} mice. We found that gene deletion of *Trpv3* attenuated the carvacrol-triggered inflammation and scaly lesions (Figure 2a, top panel; Figure 2b), and the administration of Scu (0.5 mg·kg⁻¹) did not have additional protective effect in the knockout (KO) animals (Figure 2a, top panel; Figure 2b). Deletion of *Trpv3* also suppressed the carvacrol-induced erythema and epidermal thickness by 76.8 ± 5.1% (n = 5, P < 0.05) and 62.0 ± 8.1% (n = 5, P < 0.05), respectively, and the application of Scu (0.5 mg·kg⁻¹) had no additional effect on carvacrol-induced erythema and epidermal thickness in the *Trpv3*^{-/-} mice (Figure 2c,d). Similarly, deletion of *Trpv3* abolished carvacrol-evoked itching behaviour and attenuated the increase in serum IgE level, both of which were not further improved by Scu (Figure 2e,f). Finally, the carvacrol-induced increase in mRNA expression of inflammatory cytokines, *Il-1β*, *Tnf-α*, *Il-4*, *Il-6*, and *Cxcl15* in skin lesions was far less in *Trpv3*^{-/-} than in WT mice and the application of Scu failed to affect the mRNA expression of these cytokines in the *Trpv3*^{-/-} mice (Figure 2g). These data suggest that carvacrol induces dermatitis mainly through TRPV3 activity and Scu overlaps with *Trpv3* gene deletion in suppressing the carvacrol-induced pruritus, skin inflammation and hyperplasia.

3.3 | Scu is a novel TRPV3 inhibitor

Given that Scu attenuation of carvacrol-induced dermatitis depends on TRPV3, we investigated the direct effect of Scu on mTRPV3 activity using patch-clamp recordings. In HEK-293 cells expressing mTRPV3, the application of 2-APB (100 μM) produced outwardly rectifying whole-cell currents that reached the plateau in ~20 s (Figure 3a). The currents reversed at approximately 0 mV. The much larger outward currents than inward currents likely resulted from inhibitory effects by Ca²⁺ as previously described (Xiao et al., 2008). Co-application of Scu (10 μM) strongly decreased the 2-APB-induced TRPV3 current (Figure 3a). This decreased response in the presence of Scu is unlikely due to desensitization because TRPV3 is well-known

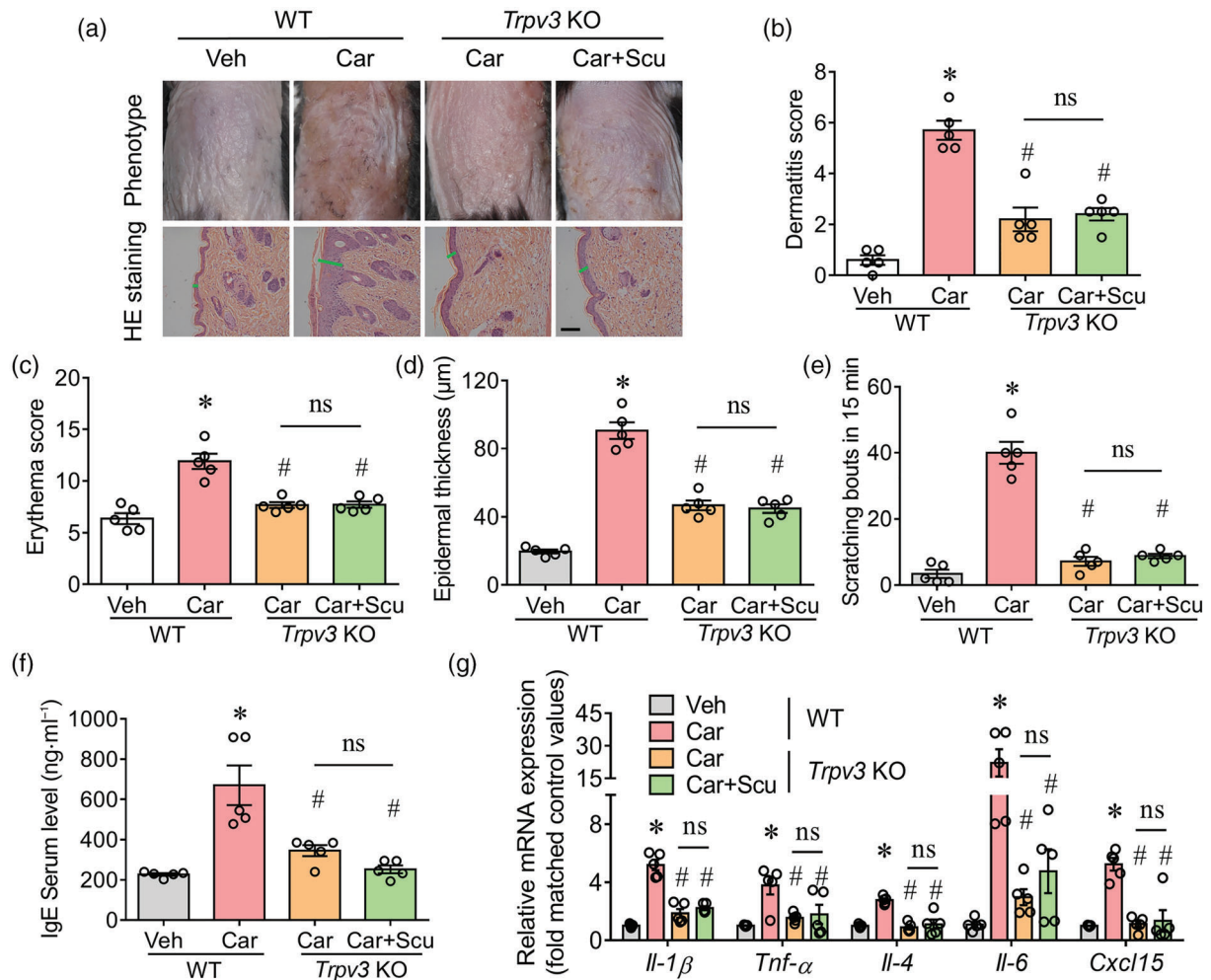


FIGURE 2 Scu suppression of carvacrol-induced dermatitis is TRPV3 dependent. (a) Representative images of the gross appearance (upper panel) and H&E-stained sections (bottom panel) of wild type (WT) mice treated with vehicle (Veh, 30% ethanol solution and saline containing 10% tween-80) and 2% carvacrol (Car), and *Trpv3* knockout (KO) mice treated with Car and Car plus Scu (0.5 mg·kg⁻¹). Black scale Bar, 50 μ m. Green lines indicate the thickness of epidermis. (b–f) Quantification of dermatitis score (b), erythema score (c), epidermal thickness (d), scratching bouts (e), and serum IgE level (f) in WT and *Trpv3* KO mice treated with Veh, Car, and Car plus Scu as indicated. (g) Relative mRNA levels of *Il-1 β* , *Tnf- α* , *Il-4*, *Il-6*, and *Cxcl15* in the lesioned skins of WT and *Trpv3* KO mice treated with Veh, Car, and Car plus Scu as indicated. Bar graphs represent mean \pm SEM (n = 5 mice). *P < 0.05 versus WT-Veh; #P < 0.05 versus WT-Car; ns, no significance versus *Trpv3* KO-Car, by one-way ANOVA followed by Dunnett's multiple comparison tests

to respond to the repeated application of 2-APB with sensitization (Peier et al., 2002). Because of the much larger current amplitude at positive potentials, we quantified the Scu effect based on the whole-cell currents recorded at +100 mV. Scu concentration-dependently decreased the response to 100 μ M 2-APB with an IC₅₀ value of 1.18 \pm 0.11 μ M (Hill coefficient = 0.84) (Figure 3b,c). The maximal inhibition of the TRPV3 current attained by Scu was ~80%. The incomplete inhibition is likely related to Scu being a negative allosteric modulator of TRPV3 (see below). Similar to the inhibition on 2-APB induced currents, Scu (30 μ M) also suppressed the carvacrol (500 μ M)-induced TRPV3 currents, by ~68% at +100 mV (Figure S2).

Using outside-out and inside-out configurations, we also tested how Scu (10 μ M) affects single channel currents evoked by 2-APB (10 μ M) (Figure 3d). In outside-out patches excised from

mTRPV3-expressing HEK-293 cells, Scu (10 μ M) suppressed the 2-APB-induced current, as shown by a decrease of the channel open probability (NP_o) at +60 mV from 0.63 \pm 0.05 to 0.15 \pm 0.04 (n = 5, P < 0.05), without altering the unitary conductance (Figure 3d–f). However, in inside-out patches, Scu had no effect on either NP_o or unitary conductance (Figure 3d–f), suggesting that Scu gains access to the mTRPV3 channel from the extracellular side. Furthermore, Scu reduced the maximal whole-cell currents evoked by 2-APB without changing the concentration dependence on the agonist (EC₅₀ for 2-APB activation of TRPV3 currents: 43.1 \pm 2.2 μ M, Hill coefficient = 1.04 without Scu versus 46.5 \pm 4.4 μ M, Hill coefficient = 1.21 with 30 μ M Scu, n = 5) (Figure 3g,h), implicating a non-competitive mechanism for Scu inhibition of the 2-APB-evoked mTRPV3 currents.

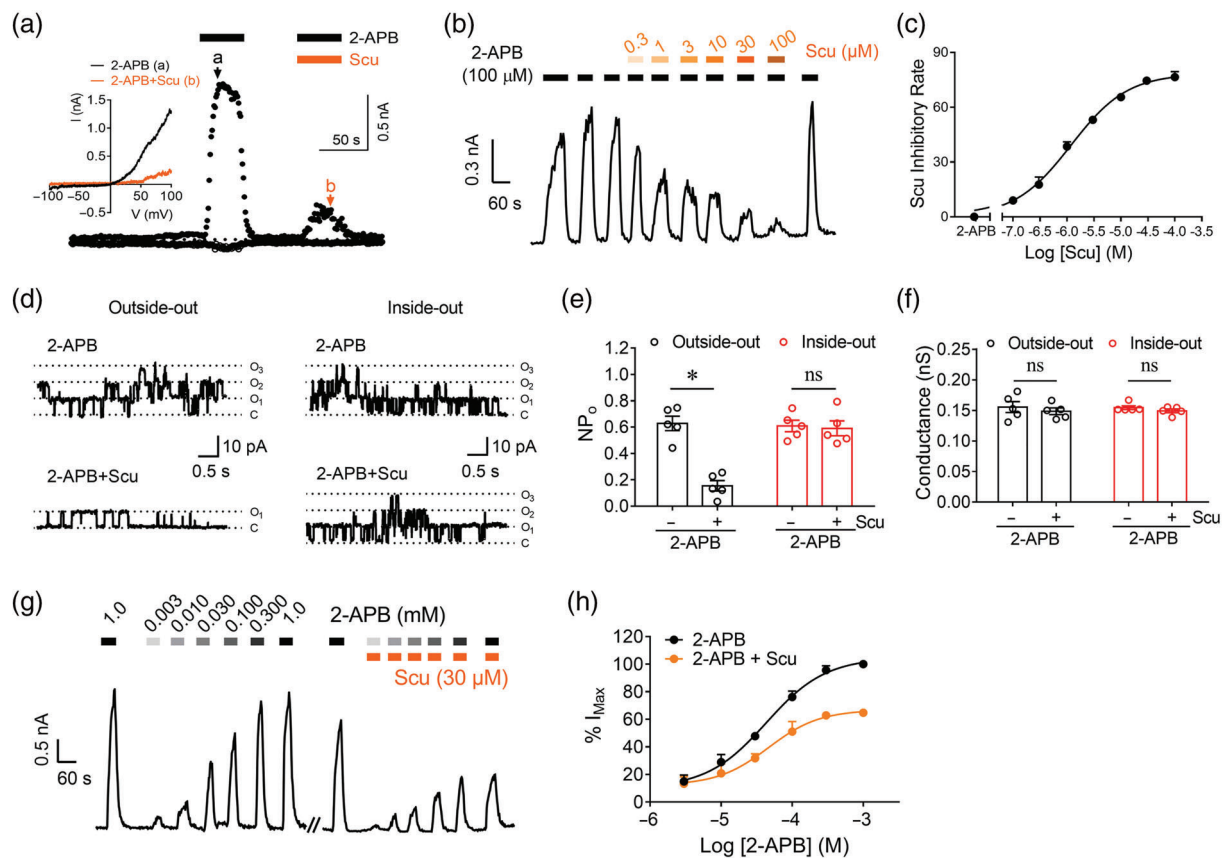


FIGURE 3 Scv inhibits 2-APB-evoked TRPV3 currents in a non-competitive fashion. (a) Representative TRPV3 current traces at ± 100 mV following bath application of 2-APB ($100 \mu\text{M}$) in the absence and presence of Scv ($10 \mu\text{M}$). Inset: I-V relationship of 2-APB-induced TRPV3 currents in the absence and presence of Scv, derived from the time points of a and b. (b) Influences of different concentrations of Scv on 2-APB-evoked TRPV3 whole-cell currents at $+100$ mV. (c) Concentration-response curve of Scv suppression of 2-APB-induced TRPV3 currents. Each data point represents mean \pm SEM ($n = 10$ cells). (d) Single-channel recording of TRPV3 currents at $+60$ mV in the presence of 2-APB ($10 \mu\text{M}$) without or with Scv ($10 \mu\text{M}$) applied through bath in outside-out (left panels) and inside-out (right panels) configurations. (e, f) Summaries of the open probabilities (NP_o) (e) and unitary conductance (f) of TRPV3 single channels upon 2-APB treatment in the absence and presence of Scv. $*P < 0.05$, ns, no significance. Paired t -test. (g) Representative traces of whole-cell currents at $+100$ mV induced by different concentrations of 2-APB in the absence and presence of Scv ($30 \mu\text{M}$) in HEK-293 cells expressing mTRPV3. (h) Concentration-response relationship curves of 2-APB-induced TRPV3 currents at $+100$ mV in the absence (black) and presence (orange) of Scv. The currents were normalized to that evoked by 1 mM 2-APB in the absence of Scv for each cell. Each data point represents mean \pm SEM ($n = 5$ cells)

3.4 | Selectivity of Scv among thermo-TRP channels

To investigate the selectivity of Scv among thermosensitive TRP channels, we tested the effect of Scv ($10 \mu\text{M}$) on whole-cell currents evoked by capsaicin, 2-APB, GSK1016790A, AITC, and menthol in HEK-293 cells that stably expressed hTRPV1, mTRPV2, hTRPV4, hTRPA1, and hTRPM8, respectively (Figure 4). Except for a slight inhibition of 2-APB-evoked TRPV2 currents by $27.6 \pm 7.4\%$ ($n = 5$, $P < 0.05$) (Figure 4b,f), Scv did not significantly affect the activation of TRPV1, TRPV4, TRPA1, and TRPM8 by their corresponding agonists (Figure 4a,c-f). Testing the concentration-response relationship of Scv on TRPV2 revealed an IC_{50} value of $10.8 \pm 2.3 \mu\text{M}$ (Hill coefficient = 0.93) ($n = 5$) (Figure S3). In a Ca^{2+} assay in HEK-293 cells expressing either hTRPV1 or mTRPV2, Scv was shown to have no detectable effect on intracellular Ca^{2+} (Figure S4), suggesting that

Scv is unable to activate either hTRPV1 or mTRPV2. These data demonstrate that Scv suppresses TRPV3 activity with at least about one order of magnitude higher potency than other thermosensitive TRP channels.

3.5 | Scv acts at the extracellular cavity formed by the transmembrane helix S6 and pore helix of TRPV3

We next explored the molecular mechanism of Scv action on TRPV3. In silico docking of Scv to the cryo-EM structure of mTRPV3 (PDB ID: 6LGP) yielded five putative binding pockets, among which, sites 1, 2 and 3 are located at the intracellular side, site 4 is within the ion permeation pathway, whereas site 5 is located at the extracellular side wedged in between the transmembrane helix S6 and pore helix (Figure 5a). That the inhibitory effect of Scv on TRPV3 was observed

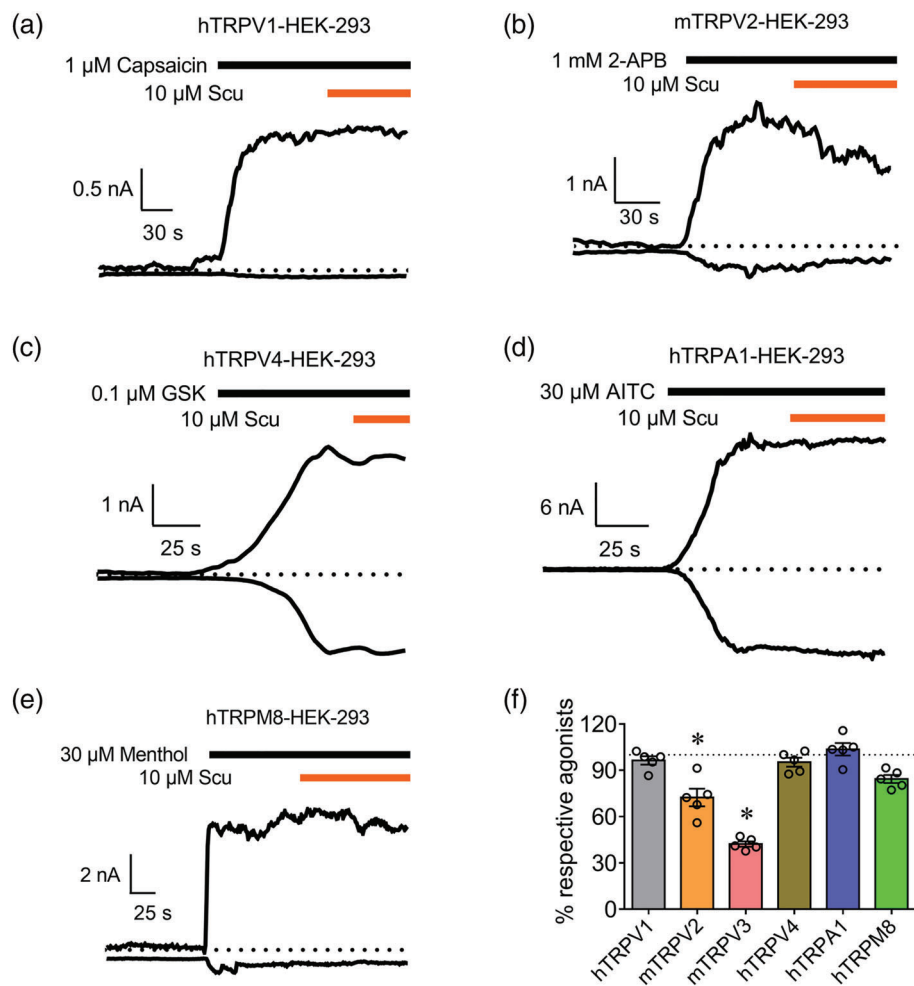


FIGURE 4 Effects of Scu on thermosensitive TRP channels. (a–e) Representative traces of whole-cell currents at ± 100 mV activated by capsaicin (1 μ M), 2-APB (1 mM), GSK1016790A (100 nM), AITC (30 μ M), and menthol (30 μ M) in HEK-293 cells stably expressing hTRPV1 (a), mTRPV2 (b), hTRPV4 (c), hTRPA1 (d), and hTRPM8 (e), respectively. Scu (10 μ M) was applied after the currents reached steady state as indicated. (f) Quantification of the inhibitory rate of Scu (10 μ M) on TRPV1, TRPV2, TRPV3, TRPV4, TRPA1, and TRPM8 whole-cell currents. Bars represent mean \pm SEM ($n = 5$ cells) of currents in the presence of 10 μ M Scu normalized to that with the respective agonist alone. * $P < 0.05$ versus respective agonist alone (indicated by the dashed line), by nonparametric Mann–Whitney test

in outside-out, but not inside-out single channel recording (Figure 3d–f) suggests that Scu likely gains access to the channel from the extracellular side, excluding sites 1–3 for Scu binding. In addition, Scu inhibited 2-APB-induced TRPV3 currents in a non-competitive manner, suggesting a negative allostery between Scu and 2-APB action. Consistent with the negative allosteric modulation, sites 4 and 5 differ from the three putative 2-APB interaction sites observed in the open cryo-EM structure of TRPV3 (Singh et al., 2018; Zubcevic & Borschel, 2019).

To clarify the Scu binding site, we systematically investigated the key amino acids involved in coordinating Scu in sites 4 and 5 by introducing mutations at the individual residues using site-directed mutagenesis. Among the mutants made in site 4, I637A, L639A, and N671A rendered the channel insensitive to 2-APB (Figure S5A–C), whereas I637L, F666A, V667I, and N671Q were functionally responsive to 2-APB, but only F666A exhibited a marked decrease in the sensitivity to block by Scu (Figure 5b,c). It should be noted that Phe⁶⁶⁶ is also a key amino acid for coordinating Scu interaction in site 5; thus, we further examined effect of site 5 mutations. Although Scu (10 μ M) suppressed 2-APB-induced currents in cells that expressed Y594I, I595A, F633A, I644W, and L655V mTRPV3 mutants similarly

as its inhibition of the WT channel, it exerted markedly reduced inhibition of the L598A, V629A, L630W, T636A, and I659F mutants (Figure 5b,c). The IC_{50} values of Scu suppression of 2-APB-induced currents were 14.7 ± 5.1 μ M (L598A), 60.2 ± 7.9 μ M (V629A), 14.3 ± 4.3 μ M (L630W), 118.5 ± 34.2 μ M (T636A), 13.6 ± 2.9 μ M (I659F) and 284.1 ± 55.3 μ M (F666A) (Figure 5d). Taken together, these results indicate that site 5, rather than site 4, is important for Scu binding that suppresses TRPV3 channel function.

To further confirm the role of site 5 in Scu inhibition of TRPV3, we substituted Ile⁶⁵⁹ and Val⁶²⁹ with Cys. Both I659C and V629C mutants of mTRPV3 were functionally responsive to 2-APB and sensitive to the inhibition by Scu (Figure 5e). However, after incubation with dithiobinitrobenzoic acid (DTNB) to introduce a 2-nitrobenzoic (NB) group that covalently modifies Cys, which in I659C or V629C would physically occupy site 5 to interfere with ligand binding, the Scu inhibition was dramatically attenuated. In I659C, the inhibition reduced from $68.7 \pm 2.3\%$ to $21.9 \pm 3.3\%$, whereas in V629C, it decreased from $62.2 \pm 1.9\%$ to $14.1 \pm 2.0\%$, respectively, by the incubation with DTNB (Figure 5e,f). As a control, DTNB did not affect Scu inhibition of WT TRPV3 channels (Figure 5e,f). Furthermore, with the subsequent application of the reducing agent, dithiothreitol (DTT),

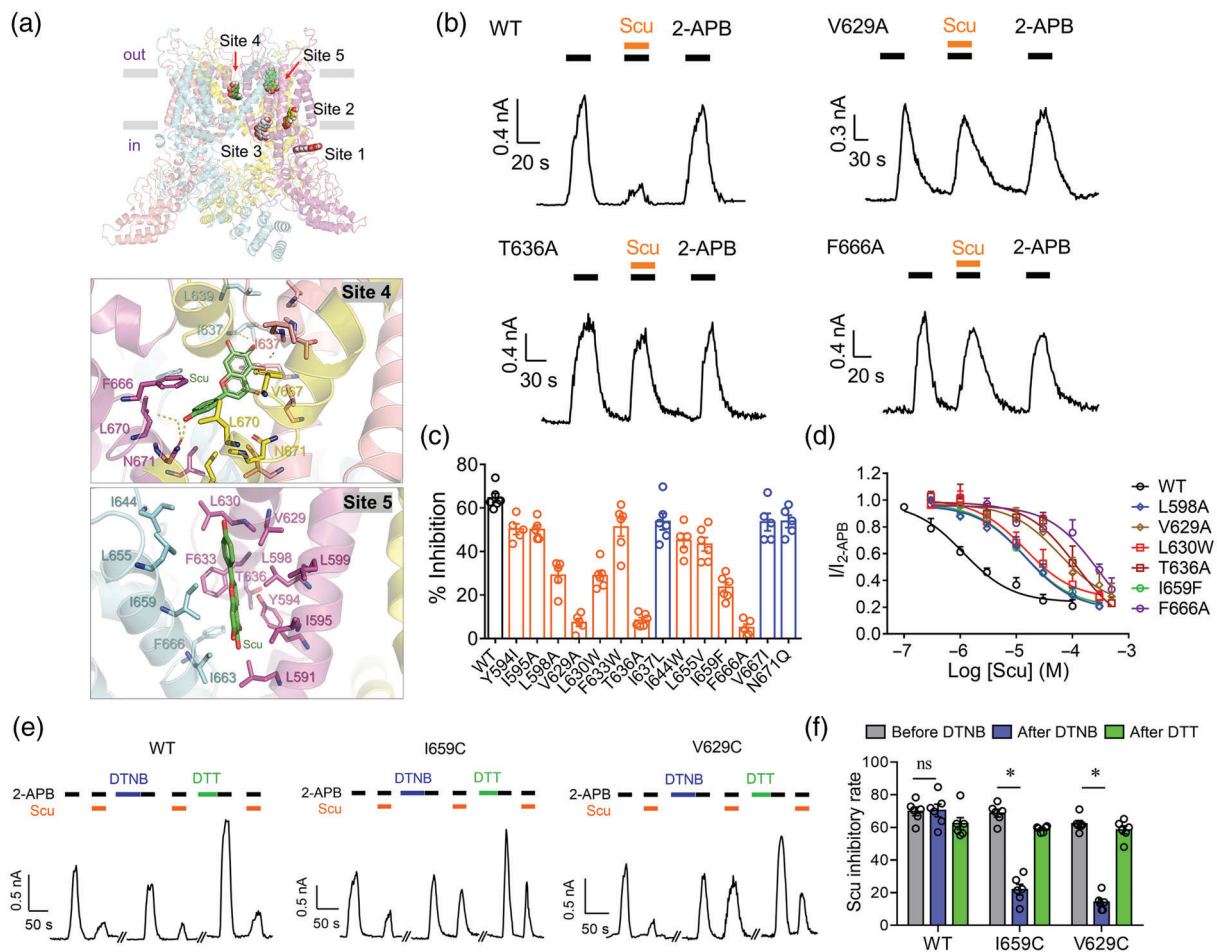


FIGURE 5 Critical amino acid residues essential for Scu inhibition on TRPV3. (a) Overall view of the mTRPV3-Scu complex. Five putative binding pockets for Scu in the mTRPV3 channel (PDB ID: 6LGP) are denoted as sites 1–5, with the zoom-in view of sites 4 and 5 shown below. (b) Representative whole-cell currents at +100 mV, showing Scu inhibition of 2-APB-induced currents in HEK-293 cells transiently expressing mTRPV3 (wild type, WT) and V629A, T636A and F666A mutants. Black (100 μ M 2-APB) and orange (10 μ M Scu) bars indicate the duration of the drug treatment. (c) Summary of Scu inhibition (%) of 2-APB-induced currents at +100 mV in cells that expressed WT mTRPV3 and mTRPV3 mutants. Blue and orange bars designate mutations at sites 4 and 5, respectively. (d) Concentration–response curves of Scu inhibition of WT mTRPV3 and its mutants. (e) Representative whole-cell recordings of 2-APB-induced currents at +100 mV in WT (left), I659C (middle) and V629C (right) mTRPV3 mutants in the absence and presence of Scu (10 μ M) before and after sequential exposures to dithionitrobenzoic acid (DTNB) and dithiothreitol (DTT). (f) Summary of Scu inhibition of 2-APB-induced currents at +100 mV of WT mTRPV3 and its I659C and V629C mutants before and after sequential exposures to DTNB and DTT. Data are mean \pm SEM ($n = 5$ cells). * $P < 0.05$; ns, no significance, by two-way ANOVA followed by Dunnett's multiple comparison tests

which should reversibly eliminate the 2-nitrobenzoic group, the Scu inhibition of 2-APB-induced current was restored in both mutants (Figure 5e,f). These data further support a mechanism of action of Scu at site 5, a cavity formed by transmembrane helix S6 and pore helix and accessible from the extracellular side.

3.6 | Scu suppresses TRPV3 channel activity in HaCaT keratinocytes

We next investigated the effect of Scu on endogenous TRPV3 activity in human skin keratinocytes, HaCaT cells. TRPV3-like whole-cell currents were induced by a TRPV3 agonist cocktail containing 2-APB (100 μ M) and carvacrol (250 μ M) as described previously (Cheng

et al., 2010), and Scu (10 μ M) inhibited the agonist cocktail-induced TRPV3-like currents at both the negative and positive potentials (Figure 6a). Quantification of the currents at +100 mV and –100 mV revealed the inhibition rates of $69.5 \pm 14.2\%$ ($n = 5$, $P < 0.05$) and $67.0 \pm 14.5\%$ ($n = 5$, $P < 0.05$), respectively (Figure 6b). The I–V curve of TRPV3 currents in HaCaT cells appeared linear, which is different from the outwardly rectifying I–V curve observed in 2-APB stimulated HEK-293 cells expressing mTRPV3 (Figure 3a). It has been reported that the development of TRPV3 currents upon continuous camphor application shifted the rectifying I–V curve to linear (Xu et al., 2005). Similarly, heat stimulation induced gradually sensitizing TRPV3 currents that changed from rectifying to a loss of rectification as the current amplitude increased (Chung et al., 2005). Such difference is likely due to the distinct open states the TRPV3 channel adapts upon

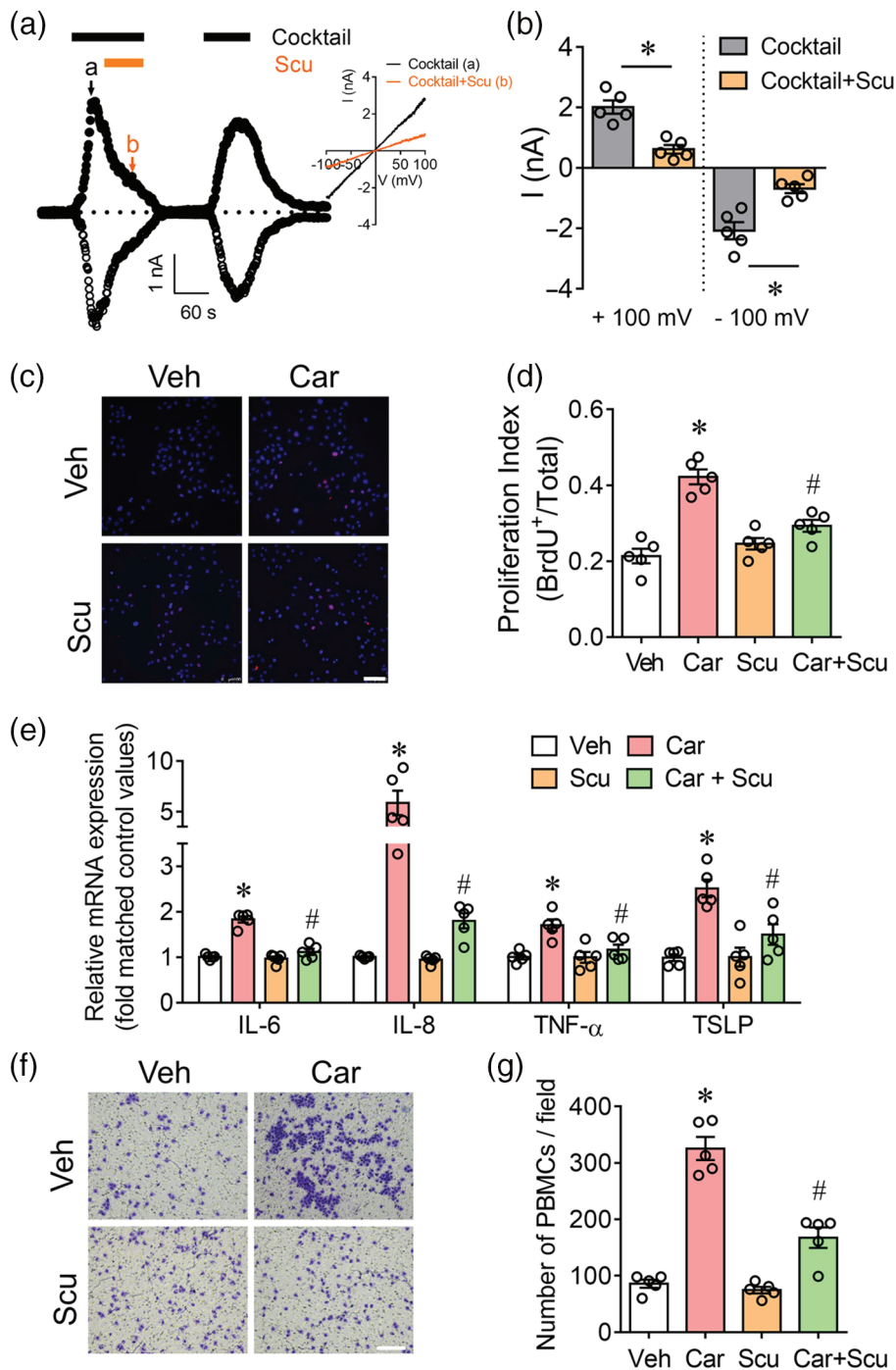


FIGURE 6 Scu inhibits carvacrol-induced cell proliferation, overexpression of proinflammatory mediators, and chemotaxis of peripheral blood mononuclear cells (PBMCs) in HaCaT keratinocytes. (a) Representative trace of whole-cell currents at ± 100 mV in HaCaT keratinocytes evoked by the agonist cocktail (100 μ M 2-APB plus 250 μ M Car) in the absence and presence of Scu (10 μ M). Inset: I-V curves for the agonist cocktail-induced currents in the absence and presence of Scu, derived from the time points of *a* and *b*. (b) Quantification of current amplitudes at ± 100 mV in HaCaT keratinocytes evoked by the agonist cocktail in the absence and presence of Scu. Data are mean \pm SEM ($n = 5$ cells). * $P < 0.05$ versus cocktail, by Student's *t*-test. (c) Representative images of BrdU-labelled HaCaT cells treated with 100 μ M Car in the absence and presence of Scu (10 μ M) for 12 h. Scale bar, 100 μ m. (d) Quantification of BrdU-positive cells after Car \pm Scu treatments. Data are mean \pm SEM from five independent experiments. * $P < 0.05$ versus Veh; # $P < 0.05$ versus Car, by one-way ANOVA followed by Dunnett's multiple comparison tests. (e) Relative mRNA levels of IL-6, IL-8, TNF- α , and TSLP in HaCaT cells treated with Car for 3 h in the absence and presence of Scu (10 μ M). Data were normalized to the vehicle (Veh) control. (f) Representative microphotographs showing fixed and stained PBMCs on the bottom side of the invasion membrane. Scale bar, 50 μ m. (g) Quantification of PBMC chemotaxis induced by media harvested from cultured HaCaT cells treated with Car in the absence and presence of Scu (10 μ M) for 6 h. Data in (d), (e), and (g) are mean \pm SEM from five independent experiments. * $P < 0.05$ versus Veh; # $P < 0.05$ versus Car, by one-way ANOVA followed by Dunnett's multiple comparison tests

treatment with different chemicals and/or a loss of divalent cation block, which contributes to the rectification behaviour (Chung et al., 2005).

3.7 | Scu suppresses carvacrol-induced proliferation and proinflammatory response in keratinocytes

Previous studies demonstrated that TRPV3 activation increases cell proliferation and IL-6 and IL-8 expression in keratinocytes (Szöllösi

et al., 2018; Wang et al., 2021). Given that Scu significantly inhibited carvacrol-triggered epidermal thickening in mice, we investigated the effect of Scu on the proliferation of HaCaT keratinocytes. A concentration of 10 μ M Scu was chosen to explore its influence on proliferation and proinflammation of keratinocytes based on its apparent affinity on TRPV3 ($IC_{50} = 1.18$ μ M). We found that Scu (10 μ M) significantly suppressed the increase in the number of BrdU-positive (BrdU $^{+}$) HaCaT cells following the treatment of carvacrol by $61.9 \pm 7.6\%$ ($n = 5$, $P < 0.05$) (Figure 6c,d), demonstrating that Scu is able to suppress the carvacrol-induced keratinocyte proliferation. Two structural analogues of Scu, baicalein (10 μ M) and chrysin (10 μ M),

which failed to inhibit agonist cocktail (10 μM 2-APB plus 10 μM carvacrol)-evoked intracellular Ca^{2+} rise in mTRPV3-expressing HEK-293 cells (Figure S6A–C), were without an effect on the carvacrol-induced cell proliferation (Figure S6D). Hispidulin (10 μM), another analog of Scu, which moderately inhibited the agonist cocktail-evoked intracellular Ca^{2+} rise in mTRPV3-expressing HEK-293 cells by $14.7 \pm 4.2\%$ (Figure S6A–C), suppressed the carvacrol-induced HaCaT cell proliferation by $42.5 \pm 11.9\%$ (Figure S6D). Analysis of the rates between inhibition of TRPV3-mediated Ca^{2+} response and suppression of carvacrol-induced keratinocyte proliferation by the Scu analogues yielded a linear correlation with correlation coefficient of 0.9194, supporting the involvement of TRPV3 in Scu inhibition of keratinocyte proliferation (Figure S6E).

Furthermore, carvacrol (300 μM) markedly increased the mRNA levels of IL-6, IL-8, TNF- α , and **thymic stromal lymphopoietin** (TSLP) to 1.83 ± 0.07 ($n = 5$, $P < 0.05$), 5.87 ± 1.21 ($n = 5$, $P < 0.05$), 1.70 ± 0.13 ($n = 5$, $P < 0.05$), and 2.51 ± 0.19 folds ($n = 5$, $P < 0.05$) of the respective controls within 3 h of the treatment (Figure 6e). Consistently, Scu (10 μM) significantly suppressed the carvacrol-induced mRNA expression of IL-6, IL-8, TNF- α , and TSLP by $86.9 \pm 8.6\%$ ($n = 5$, $P < 0.05$), $83.7 \pm 3.4\%$ ($n = 5$, $P < 0.05$), $77.0 \pm 15.7\%$ ($n = 5$, $P < 0.05$), and $66.5 \pm 14.9\%$ ($n = 5$, $P < 0.05$), respectively (Figure 6e). To confirm the effect of Scu on carvacrol-induced proinflammatory mediator release from keratinocytes, we investigated the chemotactic effects on leukocytes of the conditional medium collected from the HaCaT cell cultures. The culture medium harvested from carvacrol-treated HaCaT cells (300 μM , 6 h) significantly increased the number of chemotactic PBMCs from 86.0 ± 7.1 cells/field to 325.7 ± 20.3 cells/field ($n = 5$, $P < 0.05$) (Figure 6f,g). This effect was markedly reduced by $65.9 \pm 13.9\%$ with Scu ($n = 5$, $P < 0.05$) (Figure 6f,g). These data demonstrate that Scu suppresses carvacrol-induced cell proliferation, expression and release of chemotactic factors, and subsequently, chemotaxis of PBMCs to HaCaT keratinocytes.

4 | DISCUSSION

AD is an extensive and recrudescing cutaneous inflammatory disease with unmet clinical need. In the current study, we demonstrate that subcutaneous administration of Scu effectively inhibited pruritus, hyperplasia and cutaneous inflammation in two AD mouse models induced by carvacrol and DNFB. We further demonstrate that Scu directly inhibits TRPV3, which underlies its attenuation of pruritus, hyperplasia and cutaneous inflammation, providing the rationale and molecular basis for the use of Scu to treat cutaneous inflammatory diseases.

Previous studies have reported several structurally distinct TRPV3 inhibitors such as DPTHF (a 2-APB analog), (Pyridin-2-yl)methanol derivatives, and 26E01 (Bischof et al., 2020; Chung et al., 2005; Gomtsyan et al., 2016; Sherkheli et al., 2012), as well as endogenous metabolites including 17(R)-resolvin D1 and **isopentenyl pyrophosphate** (Bang et al., 2011, 2012), and natural compounds such as **osthole**, **forsythoside B**, **citrusinine-II**, isochlorogenic acid A and B,

monanchomycalin B, **icilin**, and urupocidin A (Han et al., 2021; Korolkova et al., 2017; Qi et al., 2021; Sun et al., 2018; Yan et al., 2019). However, potent yet selective TRPV3 inhibitors are still lacking. Among the compounds that have been subjected to TRPV3 selectivity test, osthole has been reported to attenuate DNFB-induced skin inflammation and itch through selectively inhibiting TRPV3 (Qu et al., 2019). Structurally, osthole inhibits TRPV3 activity by binding to two cavities that are shared by 2-APB. Thus, due to the conserved activity of 2-APB on TRPV1–3 channels, osthole also may act at TRPV1 and/or V2 (Neuberger et al., 2021). Indeed, osthole has been reported to be a potent TRPV1 inhibitor (Yang et al., 2016) and a **PDE4D** inhibitor (Wang et al., 2020). Inhibition of either TRPV1 or PDE4D has also been shown to attenuate itch and skin inflammation (Cohen et al., 2019; Paller et al., 2016). Moreover, (pyridin-2-yl)methanol derivatives were reported as the most potent TRPV3 inhibitors, which suppressed TRPV3 activity at sub-micromolar concentrations; however, the selectivity of this class of compounds was not reported (Gomtsyan et al., 2016). Furthermore, the naturally occurring citrusinine-II was shown to abolish pruritus through selective suppression of TRPV3 channels with an IC_{50} of 12.4 μM (Han et al., 2021). Interestingly, subcutaneous injection of a solution (50 μl) of 5 μM citrusinine-II, which would only bind to TRPV3 channels with $\sim 28\%$ receptor occupancy without considering the diffusion of compound in vivo, abolished the scratching behaviour in mice, raising doubts about the role of TRPV3 on citrusinine-II attenuation of itching and the selectivity of citrusinine-II (Han et al., 2021). In the current study, we demonstrate that Scu inhibits TRPV3 activity with a sub-micromolar potency, which is at least about one order of magnitude more potent than that on other thermo-sensitive TRP channels, providing a novel molecular tool to investigate TRPV3 function and downstream signalling pathways.

Our data demonstrate that Scu allosterically suppresses 2-APB-induced TRPV3 currents by reducing the channel's open probability. Interestingly, Scu inhibited TRPV3 activity only in outside-out recordings, but not in the inside-out configuration, suggesting that the binding pocket of Scu in TRPV3 is not accessible from the intracellular side. Consistent with this observation, in silico docking coupled with site-directed mutagenesis revealed that amino acid residues facing the cavity between the pore helix and S6 transmembrane helix, for example, Val⁶²⁹, Thr⁶³⁶, Phe⁶⁶⁶, are critical for Scu to inhibit TRPV3 channel activity. Moreover, introducing a 2-nitrobenzoic group to the engineered Cys residue at either position 659 or 629 greatly attenuated the inhibition by Scu. These data suggest that Scu acts at a pocket formed by the transmembrane helix S6 and pore helix and exposed to the extracellular surface of the TRPV3 channel, providing the molecular mechanism of Scu interaction with TRPV3. Scu may jam the movement of pore helix and S6 required for channel opening (Deng et al., 2020; Shimada et al., 2020) and thereby inhibit the TRPV3 channel activity. The same pocket has also been suggested to be critical for the inhibitory action of **dyclonine** (Liu et al., 2021) and 2,6-dimethoxy-N-(4-(4-[trifluoromethyl] phenyl)oxazol-2-yl)benzamide (Zhang et al., 2021), suggesting it being a functional “hotspot” to channel gating and allosteric negative modulation of TRPV3. This

common binding pocket differs from the two cavities bound by ost-hole, which are formed by the S1-S4 bundle and the TRP helix as well as the nexus of the linker domain and pre-S1 and TRP helices of TRPV3 (Deng et al., 2020; Singh et al., 2018; Zubcevic & Borschel, 2019).

TRPV3 channel has been shown to be a critical regulator of AD progression. Rats or mice carrying gain-of-function TRPV3 mutants develop spontaneous dermatitis and severe itch (Asakawa et al., 2005; Imura et al., 2009; Yamamoto-Kasai et al., 2013), whereas the deletion of *Trpv3* attenuates DNFB-induced skin inflammation and itch (Qu et al., 2019). In the current study, we demonstrate that deletion of *Trpv3* drastically decreased carvacrol-induced pruritus, acanthosis, and the upregulation of inflammation mediators in mice, further signifying the role of TRPV3 in the pathological progression of AD. More importantly, Scu had no additional protection against carvacrol-induced acanthosis, pruritus, and the inflammatory responses in *Trpv3* KO mice, demonstrating that Scu acts on AD phenotypes through TRPV3 channels. TRPV3 expression in keratinocytes has been reported to increase in skin lesions of AD patients (Larkin et al., 2021). Overexpression or enhanced activity of TRPV3 promotes keratinocytes to release transmitters such as NGF, prostaglandin E2 (PGE2) and TSLP, leading to itch initiation (Huang et al., 2008; Larkin et al., 2021; Seo et al., 2020). In addition, activation of TRPV3 in keratinocytes results in proinflammation responses including IL-6, IL-8 and TNF- α transcription and release (Szántó et al., 2019; Szöllősi et al., 2018). Our previous study also demonstrated that modest activation of TRPV3 enhances keratinocyte proliferation (Wang et al., 2021). In HaCaT keratinocytes, Scu suppressed carvacrol-induced cell proliferation, overexpression of chemotactic factors and proinflammatory mediators, and increased ability to recruit PBMCs by the keratinocytes. Interestingly, the ability of the flavonoid compounds to suppress keratinocyte proliferation is closely related to their inhibition of the TRPV3 function. Thus, considering the potent inhibition of TRPV3 by Scu, Scu suppression of carvacrol-induced cell proliferation and upregulation of proinflammatory factors likely occurs through direct inhibition of TRPV3 in keratinocytes. Recent studies have shown that neuronal excitation can lead to skin inflammation through releasing neuropeptides (Cohen et al., 2019; Riol-Blanco et al., 2014). Although TRPV3 is expressed in dorsal root ganglia neurons (Peier et al., 2002; Xu et al., 2002), whether neuronal TRPV3 is also involved in Scu inhibition of cutaneous inflammation and acanthosis needs further investigation. It should be mentioned that although deletion of *Trpv3* remarkably inhibited carvacrol-induced dermatitis, hyperplasia and serum IgE level, the incomplete inhibition by *Trpv3* deletion suggests the presence of an additional TRPV3-independent mechanism(s). In addition to TRPV3, carvacrol also activates TRPA1 (Suntres et al., 2015; Xu et al., 2006). Recent study has demonstrated that deletion of *Trpa1* or suppression of TRPA1 activity by HC030031 alleviated 2, 4-dinitrochlorobenzene-induced dermatitis (Zeng et al., 2021). Thus, it is likely that TRPA1 accounts for an additional component of carvacrol-induced dermatitis.

In conclusion, we demonstrate that Scu attenuates skin inflammation, pruritus and epidermal hyperplasia in mouse AD models through direct inhibition of TRPV3 by binding to an extracellularly exposed

pocket formed by the S6 transmembrane helix and pore helix. Our data not only demonstrate the molecular mechanism of Scu attenuation of AD but also identify TRPV3 as a potentially viable target for therapeutic development against AD. Given the lack of selective TRPV3 inhibitors, the potent and selective inhibition of TRPV3 by Scu also provides a useful molecular tool to study the function of TRPV3 and its downstream signalling pathways.

ACKNOWLEDGEMENTS

This work was supported by National Natural Science Foundation of China (No. 81972960, 21777192, and 82100585); National Science and Technology Major Projects for “Major New Drugs Innovation and Development” (2018ZX09101003-004-002, China); and the Joint Project between China Pharmaceutical University and East South University (2242019K3DZ01).

AUTHOR CONTRIBUTIONS

Conceptualization: Zhengyu Cao and Ye Yu; Investigation: Yujing Wang and Liaoxi Tan; Data Analysis: Qinglian Tang, Shan Jiang, Younan Ren, Chu Xue, Kejun Jiao, and Hao Chen; Writing - Original Draft Preparation: Yujing Wang, Zhao Fang, Ye Yu and Zhengyu Cao; Writing - Review and Editing: Tarek Mohamed Abd El-Aziz, Khalid N. M. Abdelazeem, Michael X. Zhu and Zhengyu Cao.

CONFLICT OF INTERESTS

The authors declare no conflict of interests.

DECLARATION OF TRANSPARENCY AND SCIENTIFIC RIGOUR

This Declaration acknowledges that this paper adheres to the principles for transparent reporting and scientific rigour of preclinical research as stated in the BJP guidelines for Design and Analysis, Natural Products, Immunoblotting and Immunochemistry, and Animal Experimentation, and as recommended by funding agencies, publishers and other organizations engaged with supporting research.

DATA AVAILABILITY STATEMENT

The data used to support the findings of this study are available from the corresponding author upon request.

ORCID

Michael X. Zhu  <https://orcid.org/0000-0002-5676-841X>
 Zhengyu Cao  <https://orcid.org/0000-0002-2692-2949>

REFERENCES

- Aijima, R., Wang, B., Takao, T., Mihara, H., Kashio, M., Ohsaki, Y., Zhang, J. Q., Mizuno, A., Suzuki, M., Yamashita, Y., Masuko, S., Goto, M., Tominaga, M., & Kido, M. A. (2015). The thermosensitive TRPV3 channel contributes to rapid wound healing in oral epithelia. *The FASEB Journal*, 29(1), 182–192. <https://doi.org/10.1096/fj.14-251314>
- Alexander, S. P., & Mathie, A. (2021). The concise guide to pharmacology 2021/22: Ion channels. *British Journal of Pharmacology*, 178(Suppl 1), S157–s245. <https://doi.org/10.1111/bph.15539>

- Alexander, S. P. H., Roberts, R. E., Broughton, B. R. S., Sobey, C. G., George, C. H., Stanford, S. C., Cirino, G., Docherty, J. R., Giembycz, M. A., Hoyer, D., Insel, P. A., Izzo, A. A., Ji, Y., MacEwan, D. J., Mangum, J., Wonnacott, S., & Ahluwalia, A. (2018). Goals and practicalities of immunoblotting and immunohistochemistry: A guide for submission to the British Journal of pharmacology. *British Journal of Pharmacology*, 175(3), 407–411. <https://doi.org/10.1111/bph.14112>
- Asakawa, M., Yoshioka, T., Hikita, I., Matsutani, T., Hirasawa, T., Arimura, A., Sakata, T., & Horikawa, T. (2005). WBN/Kob-Ht rats spontaneously develop dermatitis under conventional conditions: Another possible model for atopic dermatitis. *Experimental Animals*, 54(5), 461–465. <https://doi.org/10.1538/expanim.54.461>
- Bang, S., Yoo, S., Yang, T. J., Cho, H., & Hwang, S. W. (2011). Isopentenyl pyrophosphate is a novel antinociceptive substance that inhibits TRPV3 and TRPA1 ion channels. *Pain*, 152(5), 1156–1164. <https://doi.org/10.1016/j.pain.2011.01.044>
- Bang, S., Yoo, S., Yang, T. J., Cho, H., & Hwang, S. W. (2012). 17(R)-resolvin D1 specifically inhibits transient receptor potential ion channel vanilloid 3 leading to peripheral antinociception. *British Journal of Pharmacology*, 165(3), 683–692. <https://doi.org/10.1111/j.1476-5381.2011.01568.x>
- Bischof, M., Olthoff, S., Glas, C., Thorn-Seshold, O., Schaefer, M., & Hill, K. (2020). TRPV3 endogenously expressed in murine colonic epithelial cells is inhibited by the novel TRPV3 blocker 26E01. *Cell Calcium*, 92, 102310. <https://doi.org/10.1016/j.ceca.2020.102310>
- Borbíró, I., Lisztes, E., Tóth, B. I., Czifra, G., Oláh, A., Szöllösi, A. G., Szentandrassy, N., Nánási, P. P., Péter, Z., Paus, R., Kovács, L., & Bíró, T. (2011). Activation of transient receptor potential vanilloid-3 inhibits human hair growth. *The Journal of Investigative Dermatology*, 131(8), 1605–1614. <https://doi.org/10.1038/jid.2011.122>
- Chen, S. Y., Gao, Y., Sun, J. Y., Meng, X. L., Yang, D., Fan, L. H., Xiang, L., & Wang, P. (2020). Traditional Chinese medicine: Role in reducing β -amyloid, apoptosis, autophagy, Neuroinflammation, oxidative stress, and mitochondrial dysfunction of Alzheimer's disease. *Frontiers in Pharmacology*, 11, 497. <https://doi.org/10.3389/fphar.2020.00497>
- Cheng, X., Jin, J., Hu, L., Shen, D., Dong, X. P., Samie, M. A., Knoff, J., Eisinger, B., Liu, M. L., Huang, S. M., Caterina, M. J., Dempsey, P., Michael, L. E., Dlugosz, A. A., Andrews, N. C., Clapham, D. E., & Xu, H. (2010). TRP channel regulates EGFR signaling in hair morphogenesis and skin barrier formation. *Cell*, 141(2), 331–343. <https://doi.org/10.1016/j.cell.2010.03.013>
- Chung, M. K., Güler, A. D., & Caterina, M. J. (2005). Biphasic currents evoked by chemical or thermal activation of the heat-gated ion channel, TRPV3. *The Journal of Biological Chemistry*, 280(16), 15928–15941. <https://doi.org/10.1074/jbc.M500596200>
- Cohen, J. (1988). *Statistical power analysis for the behavioral sciences* (2nd ed.). Routledge. <https://doi.org/10.4324/9780203771587>
- Cohen, J. A., Edwards, T. N., Liu, A. W., Hirai, T., Jones, M. R., Wu, J., Li, Y., Zhang, S., Ho, J., Davis, B. M., Albers, K. M., & Kaplan, D. H. (2019). Cutaneous TRPV1⁺ neurons trigger protective innate type 17 anticipatory immunity. *Cell*, 178(4), 919–932.e914. <https://doi.org/10.1016/j.cell.2019.06.022>
- Curtis, M. J., Alexander, S., Cirino, G., Docherty, J. R., George, C. H., Giembycz, M. A., Hoyer, D., Insel, P. A., Izzo, A. A., Ji, Y., MacEwan, D. J., Sobey, C. G., Stanford, S. C., Teixeira, M. M., Wonnacott, S., & Ahluwalia, A. (2018). Experimental design and analysis and their reporting II: Updated and simplified guidance for authors and peer reviewers. *British Journal of Pharmacology*, 175(7), 987–993. <https://doi.org/10.1111/bph.14153>
- Curtis, M. J., Bond, R. A., Spina, D., Ahluwalia, A., Alexander, S. P., Giembycz, M. A., Gilchrist, A., Hoyer, D., Insel, P. A., Izzo, A. A., Lawrence, A. J., MacEwan, D. J., Moon, L. D. F., Wonnacott, S., Weston, A. H., & McGrath, J. C. (2015). Experimental design and analysis and their reporting: New guidance for publication in BJP. *British Journal of Pharmacology*, 172(14), 3461–3471. <https://doi.org/10.1111/bph.12856>
- Deng, Z., Maksaeve, G., Rau, M., Xie, Z., Hu, H., Fitzpatrick, J. A. J., & Yuan, P. (2020). Gating of human TRPV3 in a lipid bilayer. *Nature Structural & Molecular Biology*, 27(7), 635–644. <https://doi.org/10.1038/s41594-020-0428-2>
- Faul, F., Erdfelder, E., Lang, A. G., & Buchner, A. (2007). G*power 3: A flexible statistical power analysis program for the social, behavioral, and biomedical sciences. *Behavior Research Methods*, 39(2), 175–191. <https://doi.org/10.3758/bf03193146>
- Friesner, R. A., Banks, J. L., Murphy, R. B., Halgren, T. A., Klicic, J. J., Mainz, D. T., Repasky, M. P., Knoll, E. H., Shelley, M., Perry, J. K., Shaw, D. E., Francis, P., & Shenkin, P. S. (2004). Glide: A new approach for rapid, accurate docking and scoring. 1. Method and assessment of docking accuracy. *Journal of Medicinal Chemistry*, 47(7), 1739–1749. <https://doi.org/10.1021/jm0306430>
- Friesner, R. A., Murphy, R. B., Repasky, M. P., Frye, L. L., Greenwood, J. R., Halgren, T. A., Sanschagrin, P. C., & Mainz, D. T. (2006). Extra precision glide: Docking and scoring incorporating a model of hydrophobic enclosure for protein-ligand complexes. *Journal of Medicinal Chemistry*, 49(21), 6177–6196. <https://doi.org/10.1021/jm051256o>
- Gadakar, P. K., Phukan, S., Dattatreya, P., & Balaji, V. N. (2007). Pose prediction accuracy in docking studies and enrichment of actives in the active site of GSK-3beta. *Journal of Chemical Information and Modeling*, 47(4), 1446–1459. <https://doi.org/10.1021/ci6005036>
- Gomtsyan, A., Schmidt, R. G., Bayburt, E. K., Gfesser, G. A., Voight, E. A., Daanen, J. F., Schmidt, D. L., Cowart, M. D., Liu, H., Altenbach, R. J., Kort, M. E., Clapham, B., Cox, P. B., Shrestha, A., Henry, R., Whittern, D. N., Reilly, R. M., Puttfarcken, P. S., Brederson, J. D., ... Kym, P. R. (2016). Synthesis and pharmacology of (Pyridin-2-yl)methanol derivatives as novel and selective transient receptor potential Vanilloid 3 antagonists. *Journal of Medicinal Chemistry*, 59(10), 4926–4947. <https://doi.org/10.1021/acs.jmedchem.6b00287>
- Guo, F., Yang, F., & Zhu, Y. H. (2019). Scutellarein from *Scutellaria barbata* induces apoptosis of human colon cancer HCT116 cells through the ROS-mediated mitochondria-dependent pathway. *Natural Product Research*, 33(16), 2372–2375. <https://doi.org/10.1080/14786419.2018.1440230>
- Han, Y., Luo, A., Kamau, P. M., Takomthong, P., Hu, J., Boonyarat, C., Luo, L., & Lai, R. (2021). A plant-derived TRPV3 inhibitor suppresses pain and itch. *British Journal of Pharmacology*, 178(7), 1669–1683. <https://doi.org/10.1111/bph.15390>
- Harminder Singh, V., & Chaudhary, A. K. (2011). A review on the taxonomy, ethnobotany, chemistry and pharmacology of *Oroxylum indicum* vent. *Indian Journal of Pharmaceutical Sciences*, 73(5), 483–490. <https://doi.org/10.4103/0250-474x.98981>
- Huang, S. M., Lee, H., Chung, M. K., Park, U., Yu, Y. Y., Bradshaw, H. B., Coulombe, P. A., Walker, J. M., & Caterina, M. J. (2008). Overexpressed transient receptor potential vanilloid 3 ion channels in skin keratinocytes modulate pain sensitivity via prostaglandin E2. *The Journal of Neuroscience*, 28(51), 13727–13737. <https://doi.org/10.1523/jneurosci.5741-07.2008>
- Imura, K., Yoshioka, T., Hirasawa, T., & Sakata, T. (2009). Role of TRPV3 in immune response to development of dermatitis. *Journal of Inflammation (London)*, 6, 17. <https://doi.org/10.1186/1476-9255-6-17>
- Kapur, S., Watson, W., & Carr, S. (2018). Atopic dermatitis. *Allergy, Asthma and Clinical Immunology*, 14(Suppl 2), 52–52. <https://doi.org/10.1186/s13223-018-0281-6>
- Kilkenny, C., Browne, W., Cuthill, I. C., Emerson, M., & Altman, D. G. (2010). Animal research: Reporting in vivo experiments: The ARRIVE guidelines. *British Journal of Pharmacology*, 160(7), 1577–1579. <https://doi.org/10.1111/j.1476-5381.2010.00872.x>
- Korolkova, Y., Makarieva, T., Tabakmakher, K., Shubina, L., Kudryashova, E., Andreev, Y., Mosharova, I., Lee, H. S., Lee, Y. J., &

- Kozlov, S. (2017). Marine cyclic guanidine alkaloids Monanchomycalin B and Urupocidin act as inhibitors of TRPV1, TRPV2 and TRPV3, but not TRPA1 receptors. *Marine Drugs*, 15(4), 87. <https://doi.org/10.3390/md15040087>
- Langan, S. M., Irvine, A. D., & Weidinger, S. (2020). Atopic dermatitis. *Lancet*, 396(10247), 345–360. [https://doi.org/10.1016/s0140-6736\(20\)31286-1](https://doi.org/10.1016/s0140-6736(20)31286-1)
- Larkin, C., Chen, W., Szabó, I. L., Shan, C., Dajnoki, Z., Szegedi, A., Buhl, T., Fan, Y., O'Neill, S., Walls, D., Cheng, W., Xiao, S., Wang, J., & Meng, J. (2021). Novel insights into the TRPV3-mediated itch in atopic dermatitis. *The Journal of Allergy and Clinical Immunology*, 147(3), 1110–1114. e1115. <https://doi.org/10.1016/j.jaci.2020.09.028>
- Li, B., Wang, J., Cheng, X., Liu, Y., & Yu, Y. (2018). Molecular mechanism underlying the subtype-selectivity of competitive inhibitor NF110 and its distinct potencies in human and rat P2X3 receptors. *Scientific Bulletin*, 63, 1616–1625. <https://doi.org/10.1016/j.scib.2018.11.016>
- Liao, H., Ye, J., Gao, L., & Liu, Y. (2021). The main bioactive compounds of *Scutellaria baicalensis* Georgi. For alleviation of inflammatory cytokines: A comprehensive review. *Biomedicine & Pharmacotherapy*, 133, 110917. <https://doi.org/10.1016/j.biopha.2020.110917>
- Lilley, E., Stanford, S. C., Kendall, D. E., Alexander, S. P., Cirino, G., Docherty, J. R., George, C. H., Insel, P. A., Izzo, A. A., Ji, Y., & Panettieri, R. A. (2020). *ARRIVE 2.0 and the British Journal of pharmacology: Updated guidance for 2020*. Wiley Online Library.
- Lin, Y., Ren, N., Li, S., Chen, M., & Pu, P. (2019). Novel anti-obesity effect of scutellarein and potential underlying mechanism of actions. *Biomedicine & Pharmacotherapy*, 117, 109042. <https://doi.org/10.1016/j.biopha.2019.109042>
- Lin, Z., Chen, Q., Lee, M., Cao, X., Zhang, J., Ma, D., Chen, L., Hu, X., Wang, H., Wang, X., Zhang, P., Liu, X., Guan, L., Tang, Y., Yang, H., Tu, P., Bu, D., Zhu, X., Wang, K. W., ... Yang, Y. (2012). Exome sequencing reveals mutations in TRPV3 as a cause of Olmsted syndrome. *American Journal of Human Genetics*, 90(3), 558–564. <https://doi.org/10.1016/j.ajhg.2012.02.006>
- Liu, Q., Wang, J., Wei, X., Hu, J., Ping, C., Gao, Y., Xie, C., Wang, P., Cao, P., Cao, Z., Yu, Y., Li, D., & Yao, J. (2021). Therapeutic inhibition of keratinocyte TRPV3 sensory channel by local anesthetic dyclonine. *eLife*, 10. <https://doi.org/10.7554/eLife.68128>
- Logger, J. G. M., de Jong, E., Driessen, R. J. B., & van Erp, P. E. J. (2020). Evaluation of a simple image-based tool to quantify facial erythema in rosacea during treatment. *Skin Research and Technology*, 26(6), 804–812. <https://doi.org/10.1111/srt.12878>
- McGrath, J. C., McLachlan, E. M., & Zeller, R. (2015). Transparency in research involving animals: The Basel Declaration and new principles for reporting research in BJP manuscripts. *British Journal of Pharmacology*, 172(10), 2427–2432. <https://doi.org/10.1111/bph.12956>
- Miao, K., Pan, T., Mou, Y., Zhang, L., Xiong, W., Xu, Y., Yu, J., & Wang, Y. (2020). Scutellarein inhibits BLM-mediated pulmonary fibrosis by affecting fibroblast differentiation, proliferation, and apoptosis. *Therapeutic Advances in Chronic Disease*, 11, 2040622320940185. <https://doi.org/10.1177/2040622320940185>
- Möbus, L., Rodriguez, E., Harder, I., Stölzl, D., Boraczynski, N., Gerdes, S., Kleinheinz, A., Abraham, S., Heratizadeh, A., Handrick, C., Haufe, E., Werfel, T., Schmitt, J., Weidinger, S., & TREATgermany study group. (2021). Atopic dermatitis displays stable and dynamic skin transcriptome signatures. *The Journal of Allergy and Clinical Immunology*, 147(1), 213–223. <https://doi.org/10.1016/j.jaci.2020.06.012>
- Neuberger, A., Nadezhdin, K. D., Zakharian, E., & Sobolevsky, A. I. (2021). Structural mechanism of TRPV3 channel inhibition by the plant-derived coumarin osthole. *EMBO Reports*, 22(11), e53233. <https://doi.org/10.15252/embr.202153233>
- Paller, A. S., Tom, W. L., Lebwohl, M. G., Blumenthal, R. L., Boguniewicz, M., Call, R. S., Eichenfield, L. F., Forsha, D. W., Rees, W. C., Simpson, E. L., Spellman, M. C., Stein Gold, L. F., Zaenglein, A. L., Hughes, M. H., Zane, L. T., & Hebert, A. A. (2016). Efficacy and safety of crisaborole ointment, a novel, nonsteroidal phosphodiesterase 4 (PDE4) inhibitor for the topical treatment of atopic dermatitis (AD) in children and adults. *Journal of the American Academy of Dermatology*, 75(3), 494–503.e496. <https://doi.org/10.1016/j.jaad.2016.05.046>
- Peier, A. M., Reeve, A. J., Andersson, D. A., Moqrich, A., Earley, T. J., Hergarden, A. C., Story, G. M., Colley, S., Hogenesch, J. B., McIntyre, P., Bevan, S., & Patapoutian, A. (2002). A heat-sensitive TRP channel expressed in keratinocytes. *Science*, 296(5575), 2046–2049. <https://doi.org/10.1126/science.1073140>
- Percie du Sert, N., Hurst, V., Ahluwalia, A., Alam, S., Avey, M. T., Baker, M., Browne, W. J., Clark, A., Cuthill, I. C., Dirnagl, U., Emerson, M., Garner, P., Holgate, S. T., Howells, D. W., Karp, N. A., Lazic, S. E., Lidster, K., MacCallum, C. J., Macleod, M., ... Würbel, H. (2020). The ARRIVE guidelines 2.0: updated guidelines for reporting animal research. *PLoS Biology*, 18(7), e3000410. <https://doi.org/10.1371/journal.pbio.3000410>
- Qi, H., Shi, Y., Wu, H., Niu, C., Sun, X., & Wang, K. (2021). Inhibition of temperature-sensitive TRPV3 channel by two natural isochlorogenic acid isomers for alleviation of dermatitis and chronic pruritus. *Acta Pharmaceutica Sinica B*, 12, 723–734. <https://doi.org/10.1016/j.apsb.2021.08.002>
- Qu, Y., Wang, G., Sun, X., & Wang, K. (2019). Inhibition of the warm temperature-activated Ca²⁺-permeable transient receptor potential Vanilloid TRPV3 channel attenuates atopic dermatitis. *Molecular Pharmacology*, 96(3), 393–400. <https://doi.org/10.1124/mol.119.116962>
- Riol-Blanco, L., Ordovas-Montanes, J., Perro, M., Naval, E., Thiriou, A., Alvarez, D., Paust, S., Wood, J. N., & von Andrian, U. H. (2014). Nociceptive sensory neurons drive interleukin-23-mediated psoriasisiform skin inflammation. *Nature*, 510(7503), 157–161. <https://doi.org/10.1038/nature13199>
- Sánchez-Borges, M., Capriles-Hulett, A., Ortega-Martell, J. A., & Zubeldia, I. A. (2019). New and potential treatments for atopic dermatitis: Biologicals and small molecules. *Current Allergy and Asthma Reports*, 19(3), 18. <https://doi.org/10.1007/s11882-019-0849-3>
- Sárközi, S., Almássy, J., Lukács, B., Dobrosi, N., Nagy, G., & Jóna, I. (2007). Effect of natural phenol derivatives on skeletal type sarcoplasmic reticulum Ca²⁺-ATPase and ryanodine receptor. *Journal of Muscle Research and Cell Motility*, 28(2–3), 167–174. <https://doi.org/10.1007/s10974-007-9113-x>
- Seo, S. H., Kim, S., Kim, S. E., Chung, S., & Lee, S. E. (2020). Enhanced thermal sensitivity of TRPV3 in keratinocytes underlies heat-induced Pruritus release and pruritus in atopic dermatitis. *The Journal of Investigative Dermatology*, 140(11), 2199–2209.e2196. <https://doi.org/10.1016/j.jid.2020.02.028>
- Sherkheli, M. A., Gisselmann, G., & Hatt, H. (2012). Supercooling agent icilin blocks a warmth-sensing ion channel TRPV3. *The Scientific World Journal*, 2012, 982725. <https://doi.org/10.1100/2012/982725>
- Shimada, H., Kusakizako, T., Dung Nguyen, T. H., Nishizawa, T., Hino, T., Tominaga, M., & Nureki, O. (2020). The structure of lipid nanodisc-reconstituted TRPV3 reveals the gating mechanism. *Nature Structural & Molecular Biology*, 27(7), 645–652. <https://doi.org/10.1038/s41594-020-0439-z>
- Singh, A. K., McGoldrick, L. L., & Sobolevsky, A. I. (2018). Structure and gating mechanism of the transient receptor potential channel TRPV3. *Nature Structural & Molecular Biology*, 25(9), 805–813. <https://doi.org/10.1038/s41594-018-0108-7>
- Sun, X. Y., Sun, L. L., Qi, H., Gao, Q., Wang, G. X., Wei, N. N., & Wang, K. (2018). Antipruritic effect of natural Coumarin Osthole through selective inhibition of thermosensitive TRPV3 channel in the skin. *Molecular Pharmacology*, 94(4), 1164–1173. <https://doi.org/10.1124/mol.118.112466>

- Sung, N. Y., Kim, M. Y., & Cho, J. Y. (2015). Scutellarein reduces inflammatory responses by inhibiting Src kinase activity. *Korean Journal of Physiology & Pharmacology*, 19(5), 441–449. <https://doi.org/10.4196/kjpp.2015.19.5.441>
- Suntres, Z. E., Coccimiglio, J., & Alipour, M. (2015). The bioactivity and toxicological actions of carvacrol. *Critical Reviews in Food Science and Nutrition*, 55(3), 304–318. <https://doi.org/10.1080/10408398.2011.653458>
- Szántó, M., Oláh, A., Szöllösi, A. G., Tóth, K. F., Páyer, E., Czakó, N., Pór, Á., Kovács, I., Zouboulis, C. C., Kemény, L., Bíró, T., & Tóth, B. I. (2019). Activation of TRPV3 inhibits lipogenesis and stimulates production of inflammatory mediators in human Sebocytes—a putative contributor to dry skin dermatoses. *The Journal of Investigative Dermatology*, 139(1), 250–253. <https://doi.org/10.1016/j.jid.2018.07.015>
- Szöllösi, A. G., Vasas, N., Angyal, Á., Kistamás, K., Nánási, P. P., Mihály, J., Béke, G., Herczeg-Lisztes, E., Szegedi, A., Kawada, N., Yanagida, T., Mori, T., Kemény, L., & Bíró, T. (2018). Activation of TRPV3 regulates inflammatory actions of human epidermal keratinocytes. *The Journal of Investigative Dermatology*, 138(2), 365–374. <https://doi.org/10.1016/j.jid.2017.07.852>
- Vakharia, P. P., & Silverberg, J. I. (2019). Adult-onset atopic dermatitis: Characteristics and management. *American Journal of Clinical Dermatology*, 20(6), 771–779. <https://doi.org/10.1007/s40257-019-00453-7>
- Wang, S., Xie, Y., Huo, Y. W., Li, Y., Abel, P. W., Jiang, H., Zou, X., Jiao, H. Z., Kuang, X., Wolff, D. W., Huang, Y. G., Casale, T. B., Panettieri, R. A. Jr., Wei, T., Cao, Z., & Tu, Y. (2020). Airway relaxation mechanisms and structural basis of osthole for improving lung function in asthma. *Science Signaling*, 13(659). <https://doi.org/10.1126/scisignal.aax0273>
- Wang, Y., Li, H., Xue, C., Chen, H., Xue, Y., Zhao, F., Zhu, M. X., & Cao, Z. (2021). TRPV3 enhances skin keratinocyte proliferation through EGFR-dependent signaling pathways. *Cell Biology and Toxicology*, 37(2), 313–330. <https://doi.org/10.1007/s10565-020-09536-2>
- Werfel, T., Allam, J. P., Biedermann, T., Eyerich, K., Gilles, S., Guttman-Yassky, E., Hoetzenecker, W., Knol, E., Simon, H. U., Wollenberg, A., Bieber, T., Lauener, R., Schmid-Grendelmeier, P., Traidl-Hoffmann, C., & Akdis, C. A. (2016). Cellular and molecular immunologic mechanisms in patients with atopic dermatitis. *The Journal of Allergy and Clinical Immunology*, 138(2), 336–349. <https://doi.org/10.1016/j.jaci.2016.06.010>
- Wu, Y., Jin, Y., Ding, H., Luan, L., Chen, Y., & Liu, X. (2011). In-line monitoring of extraction process of scutellarein from *Erigeron breviscapus* (vant.) hand-Mazz based on qualitative and quantitative uses of near-infrared spectroscopy. *Spectrochimica Acta. Part a, Molecular and Biomolecular Spectroscopy*, 79(5), 934–939. <https://doi.org/10.1016/j.saa.2011.03.056>
- Xiao, R., Tang, J., Wang, C., Colton, C. K., Tian, J., & Zhu, M. X. (2008). Calcium plays a central role in the sensitization of TRPV3 channel to repetitive stimulations. *The Journal of Biological Chemistry*, 283(10), 6162–6174. <https://doi.org/10.1074/jbc.M706535200>
- Xu, H., Blair, N. T., & Clapham, D. E. (2005). Camphor activates and strongly desensitizes the transient receptor potential vanilloid subtype 1 channel in a vanilloid-independent mechanism. *The Journal of Neuroscience*, 25(39), 8924–8937. <https://doi.org/10.1523/jneurosci.2574-05.2005>
- Xu, H., Delling, M., Jun, J. C., & Clapham, D. E. (2006). Oregano, thyme and clove-derived flavors and skin sensitizers activate specific TRP channels. *Nature Neuroscience*, 9(5), 628–635. <https://doi.org/10.1038/nn1692>
- Xu, H., Ramsey, I. S., Kotecha, S. A., Moran, M. M., Chong, J. A., Lawson, D., Ge, P., Lilly, J., Silos-Santiago, I., Xie, Y., DiStefano, P. S., Curtis, R., & Clapham, D. E. (2002). TRPV3 is a calcium-permeable temperature-sensitive cation channel. *Nature*, 418(6894), 181–186. <https://doi.org/10.1038/nature00882>
- Yamamoto-Kasai, E., Yasui, K., Shichijo, M., Sakata, T., & Yoshioka, T. (2013). Impact of TRPV3 on the development of allergic dermatitis as a dendritic cell modulator. *Experimental Dermatology*, 22(12), 820–824. <https://doi.org/10.1111/exd.12273>
- Yan, K., Sun, X., Wang, G., Liu, Y., & Wang, K. (2019). Pharmacological activation of Thermo-transient receptor potential Vanilloid 3 channels inhibits hair growth by inducing cell death of hair follicle outer root sheath. *The Journal of Pharmacology and Experimental Therapeutics*, 370(2), 299–307. <https://doi.org/10.1124/jpet.119.258087>
- Yang, N. N., Shi, H., Yu, G., Wang, C. M., Zhu, C., Yang, Y., Yuan, X. L., Tang, M., Wang, Z. L., Gegen, T., He, Q., Tang, K., Lan, L., Wu, G. Y., & Tang, Z. X. (2016). Osthole inhibits histamine-dependent itch via modulating TRPV1 activity. *Scientific Reports*, 6, 25657. <https://doi.org/10.1038/srep25657>
- Zeng, D., Chen, C., Zhou, W., Ma, X., Pu, X., Zeng, Y., Zhou, W., & Lv, F. (2021). TRPA1 deficiency alleviates inflammation of atopic dermatitis by reducing macrophage infiltration. *Life Sciences*, 266, 118906. <https://doi.org/10.1016/j.lfs.2020.118906>
- Zhang, F., Lin, Y., Min, W., Hou, Y., Yuan, K., Wang, J., & Yang, P. (2021). Computational discovery, structural optimization and biological evaluation of novel inhibitors targeting transient receptor potential vanilloid type 3 (TRPV3). *Bioorganic Chemistry*, 114, 105093. <https://doi.org/10.1016/j.bioorg.2021.105093>
- Zhao, F., Wang, S., Li, Y., Wang, J., Wang, Y., Zhang, C., Li, Y., Huang, L., Yu, Y., Zheng, J., Yu, B., Pessah, I. N., & Cao, Z. (2021). Surfactant cocamide monoethanolamide causes eye irritation by activating nociceptor TRPV1 channels. *British Journal of Pharmacology*, 178(17), 3448–3462. <https://doi.org/10.1111/bph.15491>
- Zhao, T., Tang, H., Xie, L., Zheng, Y., Ma, Z., Sun, Q., & Li, X. (2019). Scutellaria baicalensis Georgi. (Lamiaceae): A review of its traditional uses, botany, phytochemistry, pharmacology and toxicology. *The Journal of Pharmacy and Pharmacology*, 71(9), 1353–1369. <https://doi.org/10.1111/jphp.13129>
- Zubcevic, L., & Borschel, W. F. (2019). Regulatory switch at the cytoplasmic interface controls TRPV channel gating. *eLife*, 8. <https://doi.org/10.7554/eLife.47746>

SUPPORTING INFORMATION

Additional supporting information can be found online in the Supporting Information section at the end of this article.

How to cite this article: Wang, Y., Tan, L., Jiao, K., Xue, C., Tang, Q., Jiang, S., Ren, Y., Chen, H., El-Aziz, T. M. A., Abdelazeem, K. N. M., Yu, Y., Zhao, F., Zhu, M. X., & Cao, Z. (2022). Scutellarein attenuates atopic dermatitis by selectively inhibiting transient receptor potential vanilloid 3 channels. *British Journal of Pharmacology*, 1–17. <https://doi.org/10.1111/bph.15913>